國立臺灣大學電機資訊學院電機工程學系

博士論文

Department of Electrical Engineering
College of Electrical Engineering and Computer Science
National Taiwan University
Doctoral Dissertation

多輸入單級式雙向市電併聯換流器

Multi-Input Single-Stage Bi-Directional Grid-Connected Inverter

羅國原

Kuo-Yuan Lo

指導教授：陳耀銘 博士

Advisor: Yaow-Ming Chen, Ph.D.

中華民國 105 年 7 月

July, 2016

doi:10.6342/NTU201603394

國立臺灣大學博士學位論文
口試委員會審定書

多輸入單級式雙向市電併聯換流器
Multi-Input Single-Stage Bi-Directional Grid-Connected Inverter

本論文係羅國原君（學號 D99921012）在國立臺灣大學電機工程學系完成之博士學位論文，於民國 105 年 07 月 28 日承下列考試委員審查通過及口試及格，特此證明。

口試委員：陳耀銘（簽名）
（指導教授）

賴炎生　張永瑞

邱煌仁　陳景然

系主任　劉志文（簽名）

doi:10.6342/NTU201603394

誌謝

能完成這篇論文，最要感謝的是我的指導教授陳耀銘博士，謝謝他在這六年來的悉心指導，讓我在專業領域與待人處事上獲益良多，陳老師也樹立了我研究生涯中最佳的典範，在此向陳老師致上我最誠摯的敬意與感謝。同時感謝口試委員賴炎生教授、張永瑞博士、邱煌仁教授與陳景然教授對於論文的指正與建議，在此亦致以深忱謝意。

在研究期間，感謝電能處理實驗室學長張家熙、吳政男、吳峰羽與牛元昭，實驗室同學廖建堯與陳承威，實驗室學弟陳揚霖、唐丞譽、蔡騰緯、楊景傑、陳廣哲、林瑀輝，陳要廷、陳昆宏、陳竑均、林文勳、陳彥甫、陳楷欣、李聖揚、李明學、方智煥、林鴻耀、王偵亦、陳勁延、高立桓、李佳豪與楊竣宇，實驗室學妹黃盈庭、蔡佳容、陳嘉臨與岳彤，在此同表深摯謝意。

最後，特別感謝我的父親、母親、哥哥、姐姐及老婆的支持、陪伴與關心，謹將此成果與他們分享。

doi:10.6342/NTU201603394

中文摘要

本論文提出一種新型多輸入單級式雙向市電併聯換流器。電路架構中結合多組直流-直流升降壓轉換器以及一組直流-交流展開器，由於電能轉換的過程只需要一個功率開關進行高頻切換，因此具有單級式高轉換效率特性，亦可簡化其控制器設計。當此換流器應用在市電併聯之太陽能系統時，可達到分散式最大功率點追蹤，降低遮蔽效應之影響，進而提升整體發電效益。另外，當此換流器應用在市電併聯之電池儲能系統時，可獨立控制各個低壓電池模組之充電或放電功率，同時也達到電池組間平衡與市電併聯輸出電流控制。本論文亦利用輸入電壓與脈波調變寬度來推算平均電流的方法，以取代傳統電流感測器，並實現各個轉換器輸出功率之獨立控制功能，節省整體電路成本，同時使用交錯式的開關切換方法來改善輸出電流漣波與電感尺寸。最後，透過電腦模擬與實驗結果驗證本論文所提出之換流器分別應用在太陽能系統與電池儲能系統之性能。

關鍵字：市電併聯換流器、升降壓轉換器、太陽能系統、分散式最大功率點追蹤、電池儲能系統

doi:10.6342/NTU201603394

Abstract

The objective of this dissertation is to propose a multi-input single-stage bi-directional grid-connected inverter (MSBG-inverter). The proposed MSBG -inverter is composed of multiple buck-boost type dc-dc converters (BBCs) and a dc-ac unfolder. Because there is only one switch operating at high frequency, single-stage conversion with circuit simplicity and higher efficiency can be achieved. For photovoltaic (PV) system application, the MSBG-inverters can eliminate the shading effect while fulfill the functions of dc-ac conversing and the distributed maximum power point tracking (DMPPT). For battery energy storage system application, the MSBG-inverters can realize individual power-handling capability while fulfill the functions of battery charging and discharging. Moreover, based on the developed equations, the power flow of the BBCs can be controlled without the need of input current sensor. Also, with the interleaved operation between BBCs, the current ripple of the output inductor can be reduced too. Finally, the computer simulations and hardware experimental results are shown to verify the performance of the proposed MSBG-inverter for the PV system and the battery energy storage system.

Keywords: Grid-connected inverter, buck-boost converter, PV system, DMPPT, battery energy storage system

doi:10.6342/NTU201603394

Table of Contents

doi:10.6342/NTU201603394

doi:10.6342/NTU201603394

List of Figures

doi:10.6342/NTU201603394

doi:10.6342/NTU201603394

doi:10.6342/NTU201603394

List of Tables

doi:10.6342/NTU201603394

Chapter 1 Introduction

1.1 Background

Renewable energy sources such as the photovoltaic (PV) power and wind turbines have been developed recently because of the fossil fuel exhaustion and environmental issues. In many cases, the output of the renewable energy sources such as the PV system, battery energy, and fuel cell are fluctuation DC but most of the world use AC. Therefore, the renewable energy sources based distributed generation (DG) systems are normally interfaced to the grid through power electronic converters or inverters [1] as shown in Fig. 1.1. Thus developing a grid-connected inverter system is important to use renewable energy efficiency.

The solar power market is growing stably worldwide because of the advantages of no rotating components [2]-[4]. As predicted by International Energy Agency (IEA), the PV energy will provide the electricity up to 16% of the total electricity generation by 2050 [5]. However, the output power degradation due to PV panel mismatching or shading effect as well as high installation cost becomes a hurdle [6]-[7]. One possible solution to solve the output power reduction problem is to adopt the distributed maximum power point tracking (DMPPT) configuration, which means that each PV panel should be able to produce its own maximum output power despite other PV panels' conditions. In addition, the fluctuations of the high penetration solar energy will cause the negative impact to the grid voltage and frequency stabilization because of the intermittent and uncertain characteristics. Battery energy storage system is a promising candidate to compensate the fluctuating power in the vicinity of

doi:10.6342/NTU201603394

these sources and increase the penetration rate of the renewable energy. However, the total power capacity of the battery energy storage system may be easily reduced by a particular over charging/discharging battery module due to the battery tolerance, unequal battery losses, and so on. In order to maximize energy storage, the energy of the individual battery module must be equalized with each other. Therefore, in this dissertation, a multi-input single-stage bi-directional grid-connected inverter (MSBG-inverter) is utilized to realize individual power control as well as to improve the shading effect and battery equalization for the PV system and battery energy storage system, respectively.

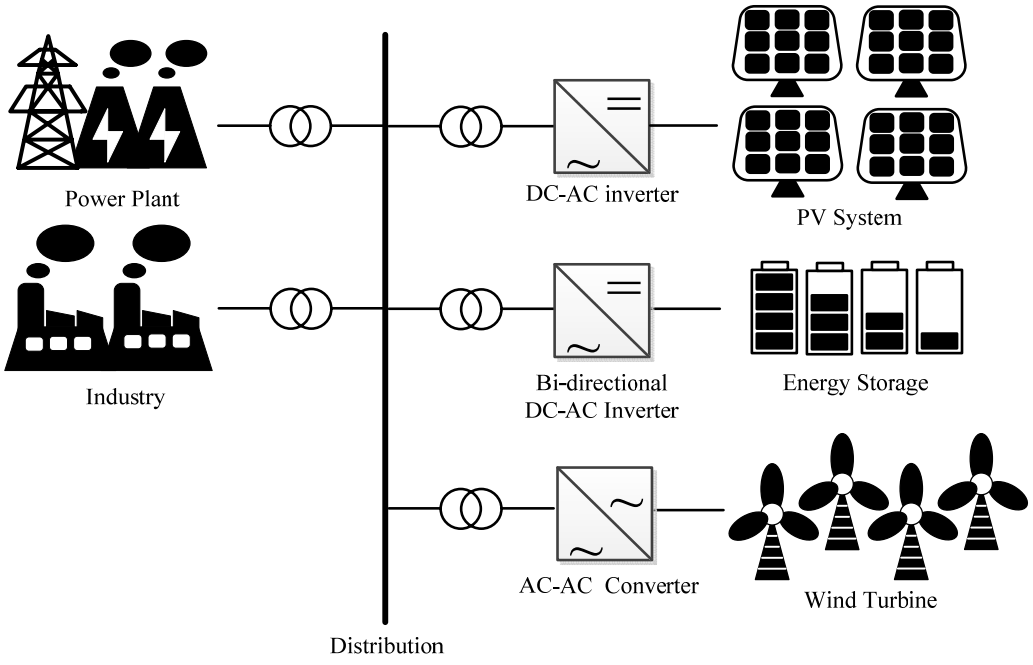

Fig. 1.1 Renewable energy based distributed power system

doi:10.6342/NTU201603394

1.2 Motivation

In general, the conventional PV power system consists of a PV array, which is formed by many PV panels connected in series or parallel, and a grid-tied dc-ac inverter [8]-[11]. The grid-tied inverter needs to perform the maximum power point tracking (MPPT) function to extract the maximum power from the PV array under different irradiance conditions [12] [13]. However, the total harvested power of the centralized PV system can be easily reduced by the PV panel mismatching, aging, or shading [14]-[17]. DMPPT is one possible solution to solve the output power reduction problem. In general, a two-stage configuration to step-up the voltage by a dc-dc converter with DMPPT function and transfer the DC power into AC power by a dc-ac inverter is necessary. Moreover, compare to the central MPPT, the main disadvantage of DMPPT is the need of many power converters, which increase the installation cost and reduce the power conversion efficiency. The expensive current sensors are required to calculate the PV output power for maximum power tracking. Both the two-stage configuration and the expensive current sensor become the major barriers for the DMPPT PV system.

For the conventional battery energy storage system, it consists of many battery modules, which is connected in series to form a high voltage input, and a bi-directional grid-tied dc-ac inverter [18]-[20]. Circuit simplicity is the main advantage of the conventional type of battery energy storage system but the total power capacity may be easily reduced by a particular over charging/discharging battery module due to the battery tolerance, unequal battery losses, and so on. In order to maximize energy storage, the charge of the individual battery module connected in series to form a dc bus as the input of the grid-tied inverter must be equalized with each other. The general solution to solve the battery capacity reduction problem is to

doi:10.6342/NTU201603394

use extra balancing circuit to connect each battery module and equalize the charge of all battery modules [21]-[23]. However, the balancing circuit may result in the reduction of total efficiency and the increase of cost and circuit complexity. Also, the battery energy storage system needs the two-stages converter to achieve the dc-ac function for the grid-connected inverter and to step-up the dc bus for charging/discharging the battery. Unfortunately, it will reduce the power conversion efficiency of the precious energy storage. The two-stages configuration and the battery module equalization are also the major barriers for the battery energy storage system.

According to the above discussion, this dissertation proposed an MSBG-inverter without using current sensors for PV system and battery energy storage system. Each PV panel or battery module has its own dc-dc converter to control the output power while the dc-ac unfolder is realized by an output inductor and four active switches operated at ac line frequency.

1.3 Dissertation Outline

This dissertation consists of six chapters. The content of each chapter is briefly described as follows.

In Chapter 2, different configurations for grid-connected inverter are first discussed. Then, the characteristics of single-stage grid-connected inverter are introduced.

In Chapter 3, the proposed MSBG-inverter is presented. The operation principle of the MSBG-inverter is first described. By deriving the mathematical equations of the proposed inverter, the output power of each DC-DC converter can be evaluated without the current sensors to realize the individual power-handling capability.

doi:10.6342/NTU201603394

Moreover, the interleaved operation is implemented to reduce the current ripple of the output inductor.

The proposed MSBG-inverter for the PV system is presented in Chapter 4. The background information of grid-connected PV system and DMPPT are first described. With the proposed current control strategy, the output power of each PV panel can be evaluated without the current sensors. Finally, computer simulations and experimental results are shown to confirm the validity of the proposed MSBG-inverter for PV system.

The proposed MSBG-inverter for battery energy storage system is presented in Chapter 5. The background information of grid-connected battery energy storage system is first described. Also, bi-directional power control and battery module equalization are considered in the proposed MSBG-inverter. Also, the interleaved operation is implemented to reduce the current ripple of the output inductor. Finally, computer simulations and experimental results are shown to confirm the validity of the proposed MSBG-inverter for battery energy storage system.

Chapter 6 summarizes the achievements of the effort and suggests further research possibilities for the future.

doi:10.6342/NTU201603394

Chapter 2 Review of Grid-Connected Inverters

In this chapter, the architecture and characteristics of different configurations for grid-connected inverter are first discussed. Based on their circuit topology, the grid-connected inverter can be divided into two categories: centralized configuration or distributed conversion configuration. In these configurations, either a two-stage converter is used for boosting the input voltage and transferring the DC power into AC power or the DC input voltage should be higher than the peak value of the grid voltage. Then, the architecture and characteristics of single-phase single-stage grid-connected inverters are introduced. After that, a summary will be given.

2.1 Centralized Configuration

According to different DC sources connection configurations, the centralized grid-connected inverter can be further divided into two types: 1.) series-connected centralized grid-connected inverter (SCG-inverter) 2.) parallel-connected centralized conversion grid-connected inverter (PCG-inverter).

2.1.1 Series Connection

In Fig. 2.1, it is shown that the SCG-inverter is formed by many voltage sources connected in series followed by a conventional grid-tied dc-ac inverter. Single-stage configuration with circuit simplicity is the main advantage of this type of grid-connected inverter system, but the total power capacity may be easily reduced due to the characteristics of different voltage source. For the PV system, the grid-tied inverter needs to perform the maximum power point tracking (MPPT) function to

doi:10.6342/NTU201603394

extract the maximum power from the PV array under different irradiance conditions. However, the total output power of this inverter system can be easily reduced by the PV panel shading or mismatching.

For the battery energy storage system, the total power capacity may be easily reduced by a particular over charging/discharging battery module due to the battery tolerance, unequal battery losses, and so on. In order to maximize the power capacity, the capacity of the individual battery module connected in series to form a dc bus as the input of the grid-tied inverter must be equalized with each other. The general solution to solve the total capacity reduction problem is to use extra balancing circuit to connect each voltage. However, the balancing circuit may result in the reduction of total efficiency and the increase of cost and circuit complexity.

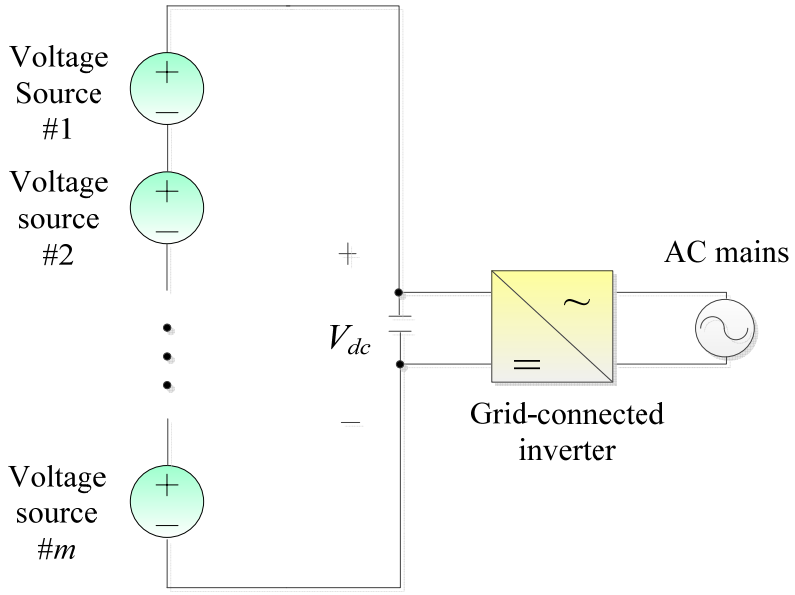

Fig. 2.1 The conceptual circuit configuration of the SCG-inverter.

doi:10.6342/NTU201603394

2.1.2 Parallel Connection

One of the ways to avoid the series connection problems of voltage sources in SCG-inverter, the PCG-inverter using a two-stage configuration to step-up the voltage by a dc-dc converter and transfer the DC power into AC power by a dc-ac inverter is shown in Fig. 2.2 [24]-[25]. For the PV system, the two-stages configuration is used for boosting the input voltage and results and transferring the DC power into AC power and may result in the reduction of total efficiency. Also, the MPPT function is difficult to be achieved for each PV panel and the total output power of this inverter system could be easily reduced by the PV panel shading or mismatching.

For the battery energy storage system, the voltage equalization of each voltage sources can be naturally achieved because of the parallel connection of each voltage source in PCG-inverter. On the other hand, it is difficult to estimate the state of charge (SOC) since it cannot measure the individual voltage of each battery module and consider the effects of the temperature and charging and discharging efficiency. Also, this inverter still implies a simpler system design with lower control complexity. However, it is lack of the individual power-handling capability required for the different types of battery module. Also, the high current stress of the dc-dc converter and an inverter as the second-stage will reduce the overall conversion efficiency. Thus the power capacity of this type of configuration is limited due to the efficiency and the current stress considerations.

doi:10.6342/NTU201603394

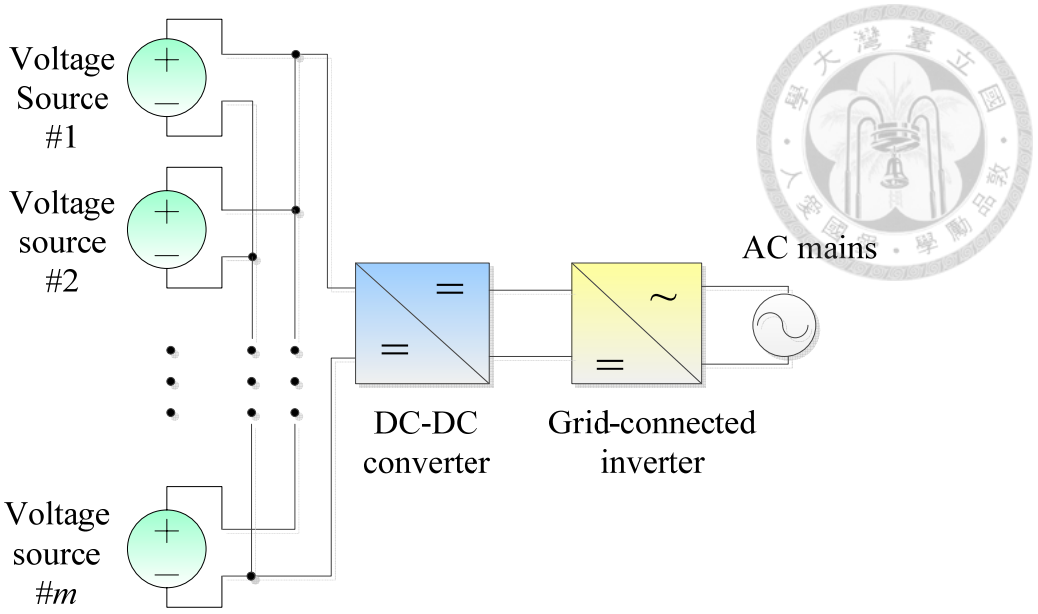

Fig. 2.2 The conceptual circuit configuration of the PCG inverter.

2.2 Distributed Conversion Configuration

Compare to the centralized configuration, the distributed conversion configuration can offer the individual power-handling capability for each voltage sources. According to the power converter configuration, the distributed conversion configuration can be further divided in three categories: 1.) series-connected distributed conversion grid-connected inverter (SDCG-inverter) 2.) parallel-connected distributed conversion grid-connected inverter (PDCG-inverter) 3.) cascade-type distributed conversion grid-connected inverter (CDCG-inverter) 4.) Micro-inverter.

2.2.1 Series Connection

Fig. 2.3 shows the SDCG-inverter where a dc-dc converter is attached to each voltage source and the output of each dc-dc converter is connected in series to form a dc bus as the input of the grid-tied inverter [26]-[28]. Each voltage source has its own dc-dc converter so the fail voltage source will not affect the output power of other

doi:10.6342/NTU201603394

voltage sources. For the PV system, the MPPT function can be achieved to extract the maximum power from each PV panel. Since the output terminal of each dc-dc converter is connected in series, low voltage rating components can be adopted and converter cost can be reduced. However, due to the unbalance power flow problems, the bi-directional power flow control of those series connected dc-dc converters is complicated and an auxiliary communication facility is needed. Also, the reliability of this inverter system may be reduced.

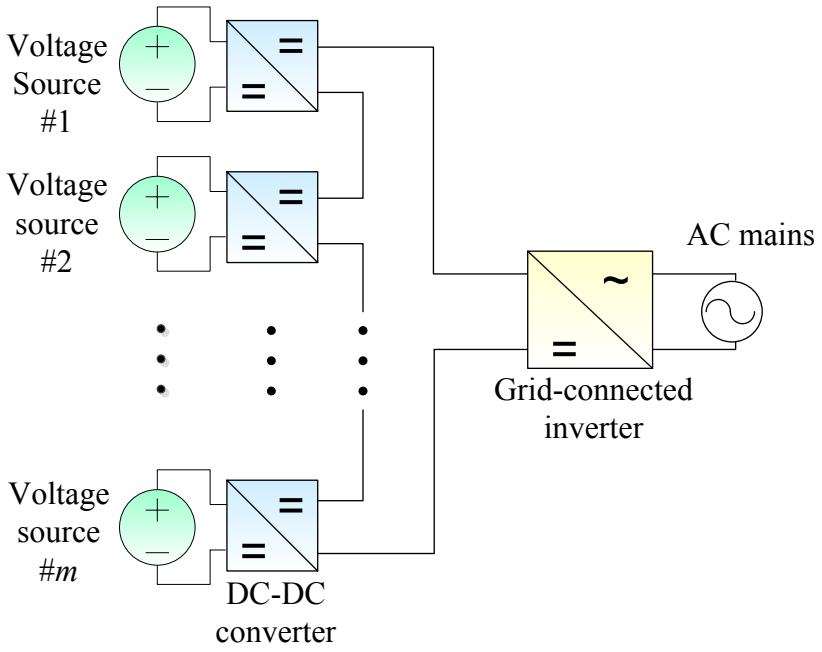

Fig. 2.3 The conceptual circuit configuration of the SDCG inverter.

2.2.2 Parallel Connection

Another configuration is PDCG-inverter as shown in Fig. 2.4. Each voltage source is connected by an individual converter and the parallel connected output terminals deliver power through a grid-tied inverter to the grid [29]. Because of the parallel connection structure, the advantages of this inverter include circuit simplicity, and individual power control for each voltage source. Therefore, the DMPPT function

doi:10.6342/NTU201603394

for the PV system, equalization for the battery energy storage system, and capacity flexibility of this inverter system can be achieved. However, these dc-dc converters with current sensors may result in the increase of cost and a second-stage dc-ac inverter is still necessary. In this dissertation, an MSBG-inverter extended from the configuration of PDCG-inverter is proposed and the above disadvantages can be improved.

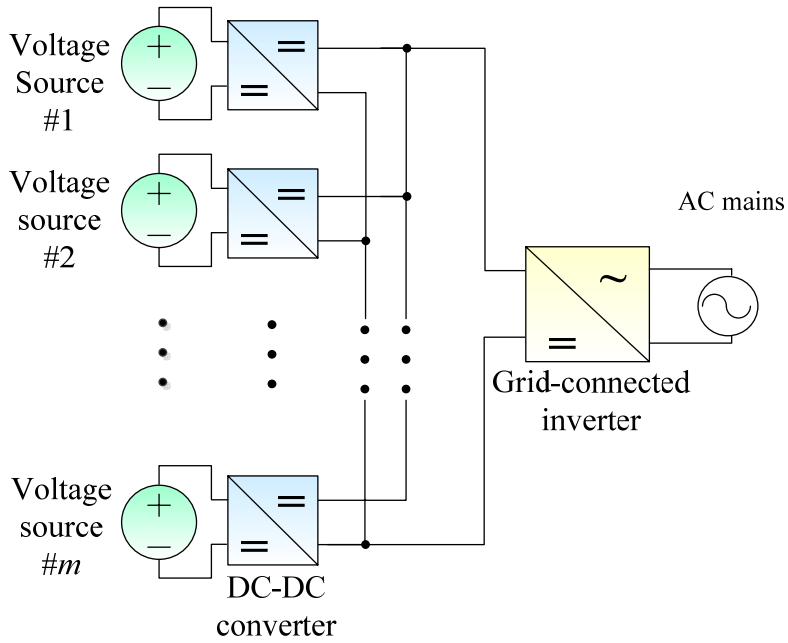

Fig. 2.4 The conceptual circuit configuration of the PDCG inverter.

2.2.3 Cascade-Type Configuration

Fig. 2.5 shows the cascade-type CDCG-inverter where the output terminals of the inverter are connected in series [30]-[31]. Compared to other configurations, cascade-type offers more flexibility and fault tolerance with multilevel topologies. Since low voltage rating components can be adopted with single-stage conversion, the inverter efficiency and cost can be improved.

For the PV system, the CDCG-inverter has the individual power-handling

doi:10.6342/NTU201603394

capability to achieve DMPPT, no limitation on the number of cascaded PV panels. Also, the CDCG-inverter is suitable to realize the bi-directional power control and equalization for the battery energy storage system. However, the control of those series connected dc-ac inverters is complicated and an auxiliary communication facility is needed.

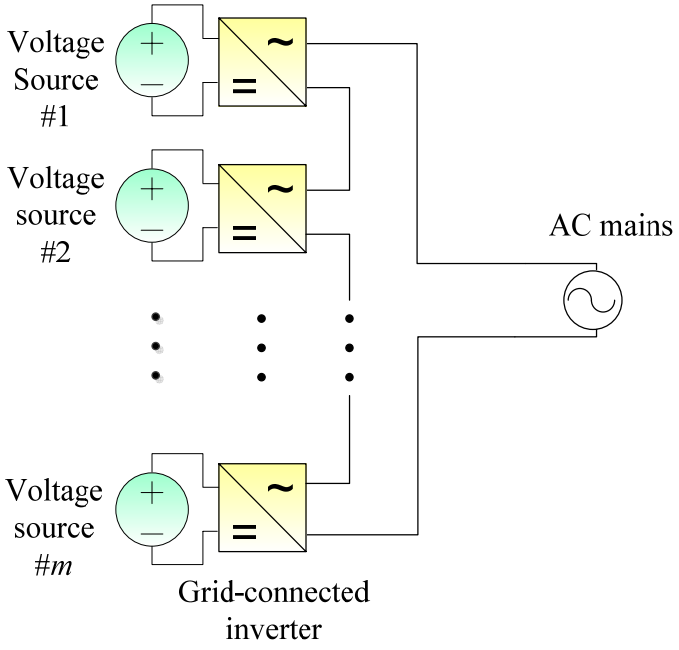

Fig. 2.5 The conceptual circuit configuration of the CDCG inverter.

2.2.4 Micro-Inverter Configuration

An alternative configuration is to adopt a dc-ac micro-inverter for each voltage source as shown in Fig. 2.6. [32-34] Compared to the above configuration, the micro-inverter offers more flexibility and fault tolerance in battery energy storage system. Since each voltage source has its own grid-connected micro-inverter, the output power of the voltage source can be individually controlled in despite of other voltage source mismatching. However, many challenges still remain in the way of achieving lower cost and higher conversion efficiency.

doi:10.6342/NTU201603394

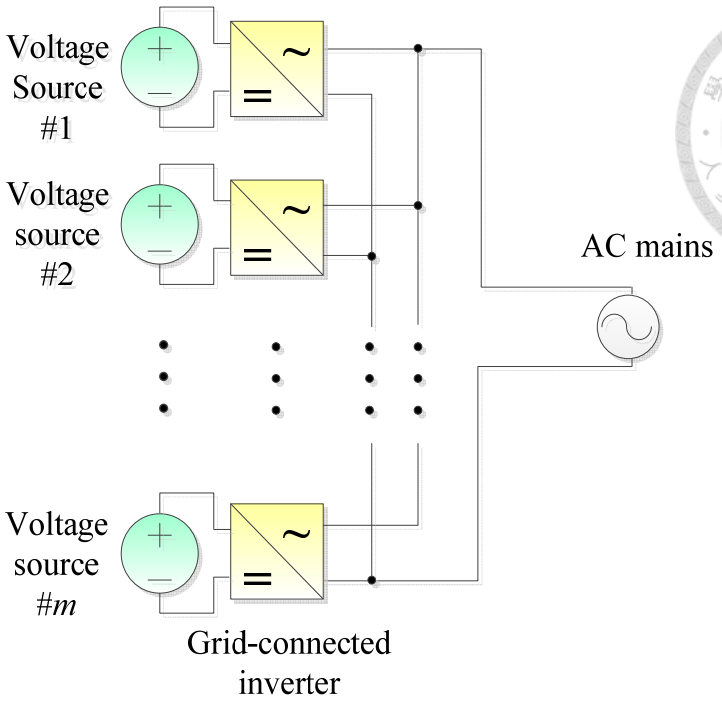

Fig. 2.6 Micro-inverter.

2.3 Single-Stage Grid-Connected Inverter

Consider of the dc-ac inverter without the DC fluctuation, the single-stage grid-connected inverter becomes a popular configuration for improving the conversion efficiency and control circuit simplicity. For the single-phase inverter, the commonly used bidirectional inverter topology consists of four power switches (H-bridge inverter) as shown in Figure 2.7. However, the input voltage will be required to be higher than the peak of the grid voltage. Also, this topology has higher switching and conduction losses in high-voltage high-power applications. Therefore, many literatures focus on developing single-stage grid-connected inverter. In this section, four main single-stage grid-connected inverter circuits are introduced and analyzed.

doi:10.6342/NTU201603394

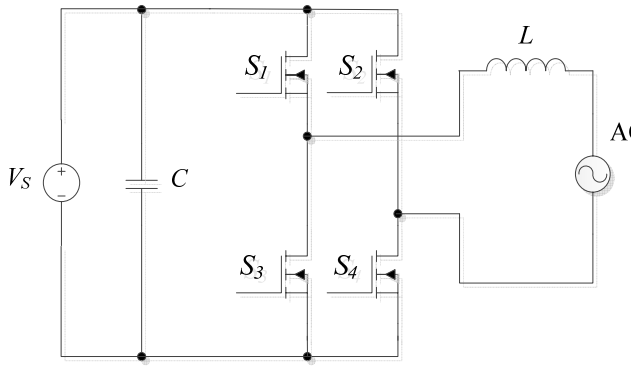

Fig. 2.7 Conventional four-switch inverter.

2.3.1 Three-Level Inverter

The three-level inverter with neutral-point-clamped (NPC) PWM topology shown in Fig. 2.8 was first introduced by Nabae, et al., in 1980 [35]-[36]. During the positive cycle of the grid, S_1 is turned on and S_2 is switched in sinusoidal pulse width modulation (SPWM). On the other hand, during the negative cycle of the grid, S_4 is turned on and S_3 is switched in SPWM. Voltages across the switches are only half of the input DC voltage. Because the midpoint of the DC-link capacitors is connected to the neutral of the grid, the leakage current is also reduced for renewable energy system application. Moreover, the principles of this three-level inverter topology can be extended to multi-level inverters with any number of levels. The multi-level inverters have better fault-tolerant ability by its modular design, so it is very suitable to produce a higher-voltage output using these low-voltage PV panels or battery modules. The output of this inverter is multilevel ac voltages where the number of levels is proportional to the number of PV panels or battery cells and that may result in the limitation of the power conversion efficiency and capacity flexibility. Also, the static and dynamic sharing of the voltage across the switches and the input capacitors is difficult and the reliability of this inverter may be reduced.

doi:10.6342/NTU201603394

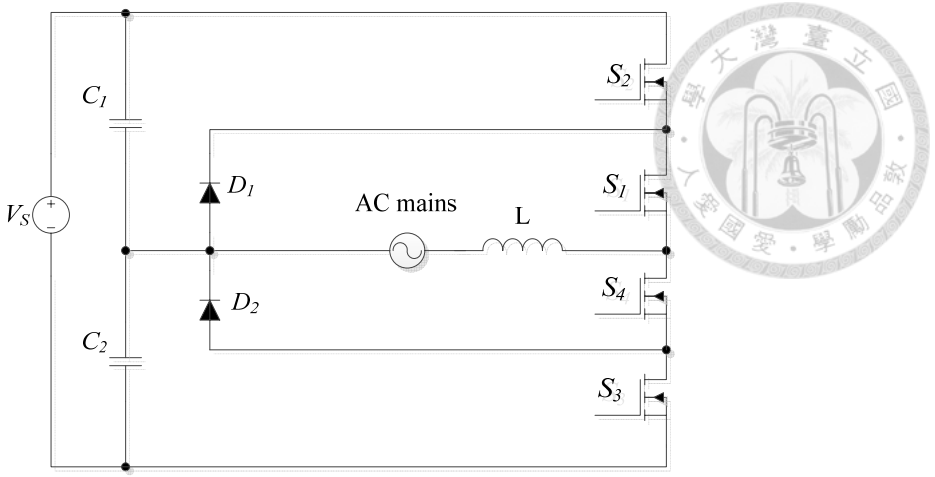

Fig. 2.8 Three-level inverter.

2.3.2 SMA H5^{TM} Inverter

Compare to the H-bridge inverter, the H5^{TM} inverter which is shown in Fig. 2.9 has drawn many attentions for the single-stage grid-connected inverter because of its higher efficiency, smaller size, and leakage current reduction [37]. In Fig. 2.9, S_1 and S_2 are switched at the ac line frequency as a low frequency selection network. During the positive cycle of the grid, S_5 and S_4 are switched in SPWM. On the other hand, during the negative cycle of the grid, S_5 and S_3 are switched in SPWM. The fast recovery diode for S_1 and S_2 is used to reduce reverse recovery loss. Since the S_5 and S_3 or S_4 share the input DC voltage, lower voltage rating components can be adopted and high conversion efficiency is achieved. Moreover, there is lower leakage current in this inverter and it's important for renewable energy system application. However, as the H-bridge inverters, the input DC voltage must higher than the peak of the grid voltage, which limits the input voltage range for renewable energy system application.

2.3.3 HERIC Inverter

Similar to the H-bridge inverter, the HERIC inverter with lower leakage current

doi:10.6342/NTU201603394

is proposed [38]. As shown in Fig. 2.10, the HERIC inverter combines the advantages of H-bridge inverter and reduces the leakage current by using auxiliary switches (S_5 and S_6) for zero states or freewheeling period. During the positive cycle of the grid, S_1 and S_4 are switched in SPWM. On the other hand, during the negative cycle of the grid, S_2 and S_3 are switched in SPWM. The auxiliary switch S_5 and S_6 are switched during freewheeling period of the positive cycle and the negative cycle, respectively. Although the frequency of the output current is equal to the switching current, this inverter generates lower leakage current with high conversion efficiency. Similar to H-bridge inverters, the input DC voltage must higher than the peak of the grid voltage.

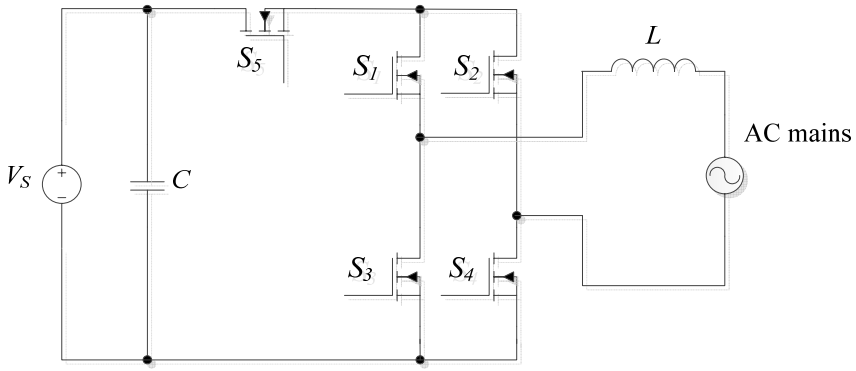

Fig. 2.9 SMA H5^{TM} inverter.

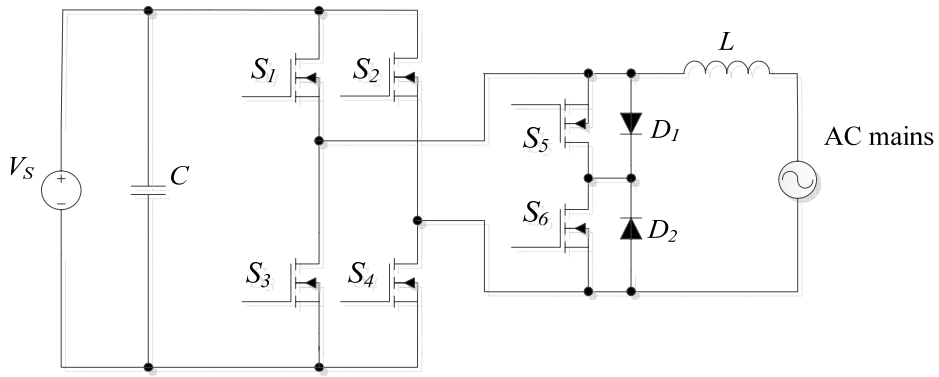

Fig. 2.10 HERIC inverter.

doi:10.6342/NTU201603394

2.3.4 Dual-Buck Inverter

In the H-bridge inverter topology, there is shoot-through issue because the active power switches are connected in series in each phase leg. A dual-buck inverter consists of two buck converters and also has features of the conventional half-bridge inverter is shown in Fig. 2.11 [39]. By using one switch at one time, not only the switching loss but also the conduction loss can be significantly reduced. The converter exhibits two distinct merits: first, there is no shoot-through issue because no active power switches are connected in series in each phase leg; second, the reverse recovery dissipation of the power switch is greatly reduced because there is no freewheeling current flowing through the body diode of power switches. The converter works as a rectifier when the power is transferred from ac grid to dc source. Alternately, it works as an inverter when the power is transferred from dc source to ac grid.

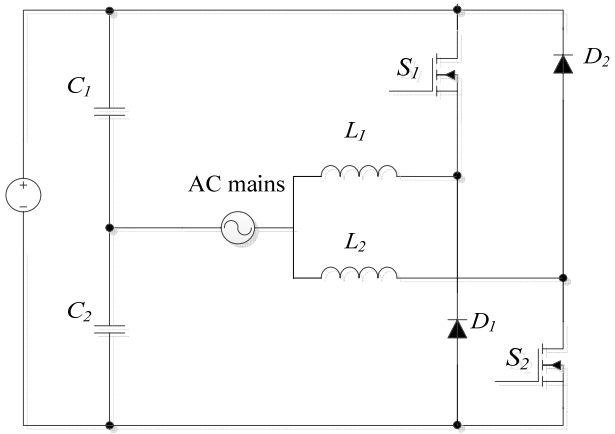

Fig. 2.11 Dual-Buck inverter.

2.4 Summary

In this section, the architecture and characteristics of different configurations for grid-connected inverter are reviewed and four main single-stage grid-connected

doi:10.6342/NTU201603394

inverter circuits are introduced. Table 2.1 lists the Comparisons of different configurations for grid-connected inverter. For these configurations, either a two-stage converter is used for boosting the input voltage and transferring the DC power into AC power or the input voltage will be required to be higher than the peak of the grid voltage. Moreover, expensive current sensors for each voltage source are required to calculate the input power for the power flow control. Both the two-stage configuration and the expensive current sensor become the major barriers for grid-connected inverter.

Therefore, this dissertation proposes an MSBG-inverter without using current sensors is proposed, as shown in Fig. 2.12, for the renewable energy system. Similar to the PDCG-inverter, the proposed MSBG-inverter can achieve individual power control of each voltage source so that important features of the DMPPT, the battery module equalization, and capacity flexibility can be accomplished. In addition, a dc-ac unfolder that only switches at the zero crossing of the line voltage is used for converting the high frequency pulsating dc current generated by the dc-dc converter into a sinusoidal one with grid frequency. Its switching loss can be neglected by comparing to those power switches in the dc-dc converter. Therefore, the energy of each voltage source is transferred to the ac mains by means of single-stage power conversion. Also, the proposed MSBF-inverter generates lower leakage current because of the unfolder. Moreover, the buck-boost dc-dc converters operated with interleaving are used to reduce the current ripple of the output inductor.

The aim of proposed inverter is to improve the power conversion efficiency, reduce the output inductor size, eliminate the input current sensor, and simplify the control circuit. Thorough analysis and mathematical equations of the proposed inverter will be presented in the next chapter.

doi:10.6342/NTU201603394

Table 2.1 Comparisons of different configurations for grid-connected inverter

Configuration		Individual power-handling (DMPPT)	Features
Centralized Conversion	SCG-inverter	No	Circuit simplicity, lower cost, and higher efficiency
	PCG-inverter	No	Voltage equalization and low efficiency with high current stress
Distributed Conversion	SDCG-inverter	Yes	Low voltage stress and circuit complexity for auxiliary communication
	PDCG-inverter	Yes	Control simplicity and lower efficiency
	CDCG-inverter	Yes	Multi-level output and control complexity
	Micro-inverter	Yes	Flexible design for expansion and higher cost

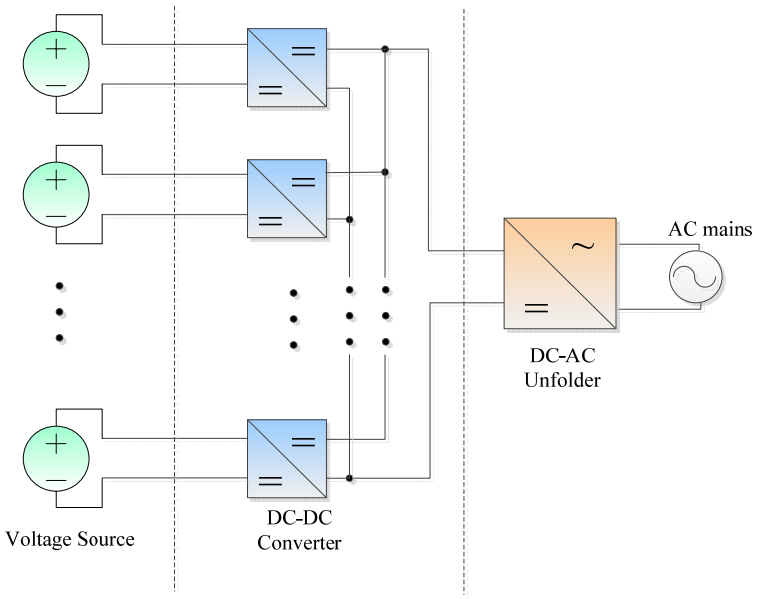

Fig. 2.12 The proposed MSBG-inverter.

doi:10.6342/NTU201603394

Chapter 3 The Proposed MSBG-Inverter

In order to improve the conversion efficiency and control circuit simplicity of grid-connected inverters, an MSBG-inverter without using current sensors is proposed in this dissertation. The circuit diagram of the proposed MSBG-inverter, which is composed of m sets of distributed buck-boost type dc-dc converters (BBCs) and a dc-ac unfolder, is shown in Fig. 3.1. Each BBC consists of two switches, two diodes, and one inductor. It can convert the DC current provided by the DC voltage source into a high frequency pulsating one with a low frequency rectified sinusoidal envelop. This high frequency pulsating output current of the BBCs will be converted into sinusoidal one with utility line frequency by the dc-ac unfolder. The dc-ac unfolder is composed of 4 active switches operated at low switching frequency and an output inductor. During the positive half-cycle of the ac mains, the switches S_A and S_D are turned-on while S_B and S_C are off. For the negative half-cycle, switches S_B and S_C are on and S_A and S_D are off. Because the unfolder only switches at the zero crossing of the grid voltage, its switching loss can be neglected by comparing to those power switches in the dc-dc converter. Therefore, the energy of each voltage source is transferred to the ac mains by means of single-stage power conversion. In this chapter, phase-lock loop (PLL) for synchronization is first described. To achieve the bi-directional power flow feature of the MSBG-inverter, two main operation modes of the BBCs will be discussed: (1) DC-AC conversion mode and (2) AC-DC conversion mode. Also, the BBCs operated with interleaving to reduce the current ripple of the output inductor are discussed.

doi:10.6342/NTU201603394

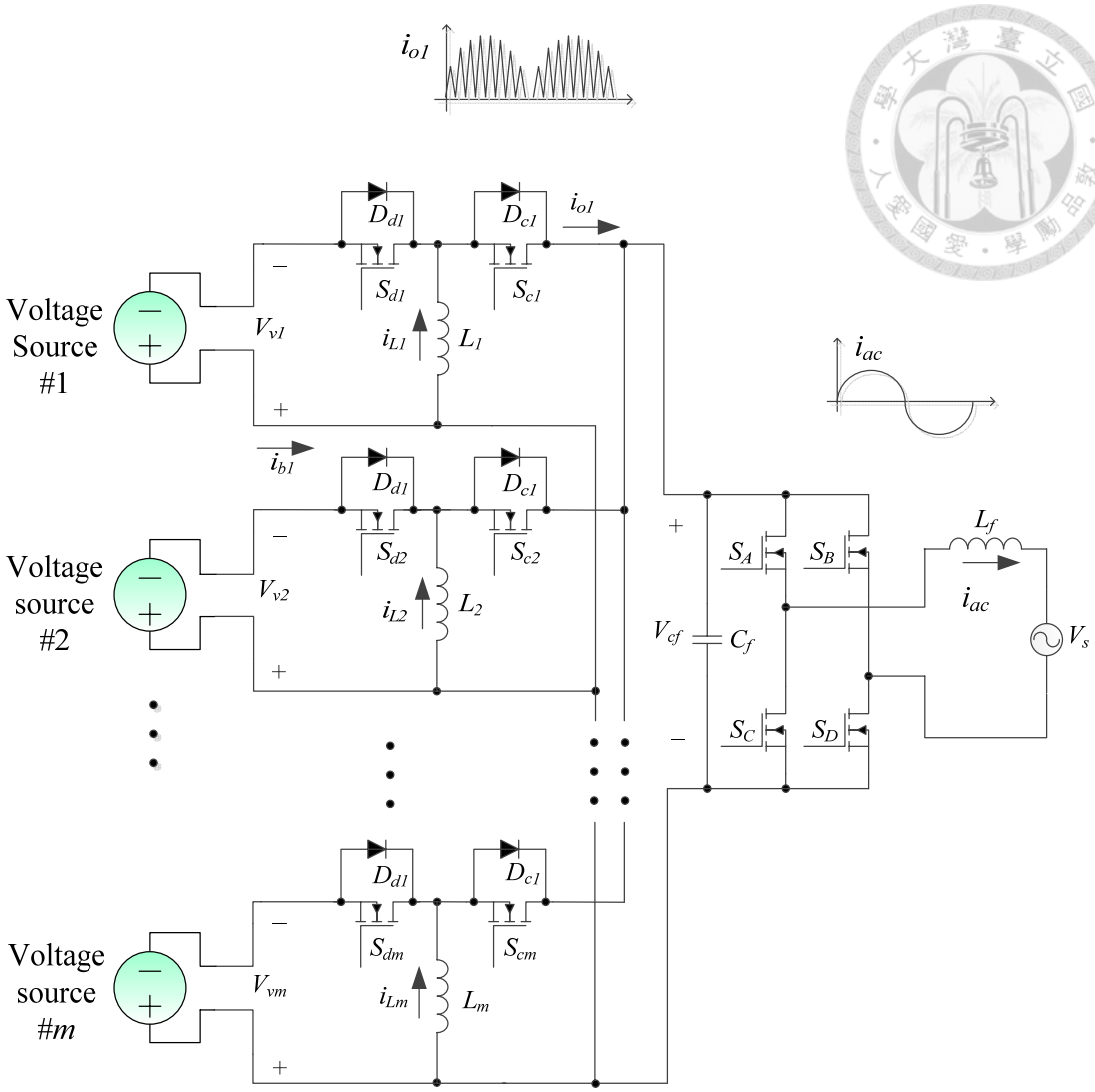

Fig. 3.1 The circuit diagram of the proposed MSBG-inverter.

3.1 Phase-Lock Loop for Synchronization

For grid-connected inverter, the synchronization is an important function and the zero-cross detection is a simple way to calculate the phase angle [40]. However, this method is sensitive to the distorted grid voltage and tends the larger steady-state error. Therefore, digital PLL is widely used because of the flexibility and high reliability for the synchronization [41]-[42]. Fig. 3.2 shows the simplified structure of the PLL controller, which is used to synchronize the phase angle of the grid. For the simplified

doi:10.6342/NTU201603394

PLL to operate, the grid measurement must have a magnitude of one that can be obtained by using the all pass filter (APF) and trigonometric identity. By using the products of the cosine of the grid angle θ_o and the sine of the PLL output angle θ_s, the product signal can be derived as:

$$V_e = \frac{1}{2}[\sin(\theta_o + \theta_s) - \sin(\theta_o - \theta_s)] \tag{3.1}$$

If $\theta_o = \theta_s + \lambda$, then (3.1) can be rewritten as:

$$V_e = \frac{1}{2}[\sin(2\theta_s) - \sin(\lambda)] \tag{3.2}$$

The low pass filter (LPF) needs to be designed to significantly attenuate the two times of the grid frequency so only sin(λ) is left. Through the LPF, K_p compensator chosen for the maximum bandwidth and a sufficient step response, and the integration of adding the grid frequency ω_f, the second harmonic term will be filtered and the PLL output angle θ_s which is used to control the output current of MSBG-inverter can be obtained as:

$$\theta_s = \int (K_p \Delta\omega + \omega_f) \tag{3.3}$$

The PLL is important to meet the requirement to synchronize with the grid for electric grid connection and it allows small variations between frequency, phase, and magnitude transients. The simplified transfer function for PLL is expressed as:

$$T_{PLL}(s) = \frac{K_p \omega_c}{s(s + \omega_c)} \tag{3.4}$$

Fig. 3.3 shows the Bode plot of the PLL controller at K_p = 250 and the cut-off frequency of *LPF* f_c = 20Hz. The PLL controller is designed to achieve a crossover frequency of 24.8 Hz in grid-connected mode and a phase margin of 34.7 degree with stability.

doi:10.6342/NTU201603394

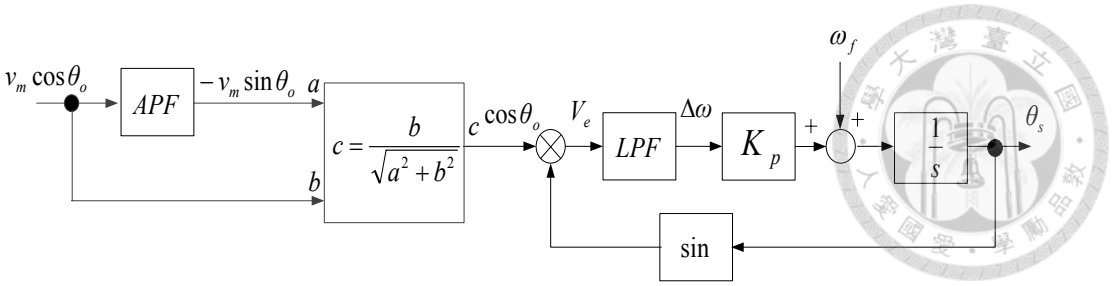

Fig. 3.2 Block diagram of the PLL controller.

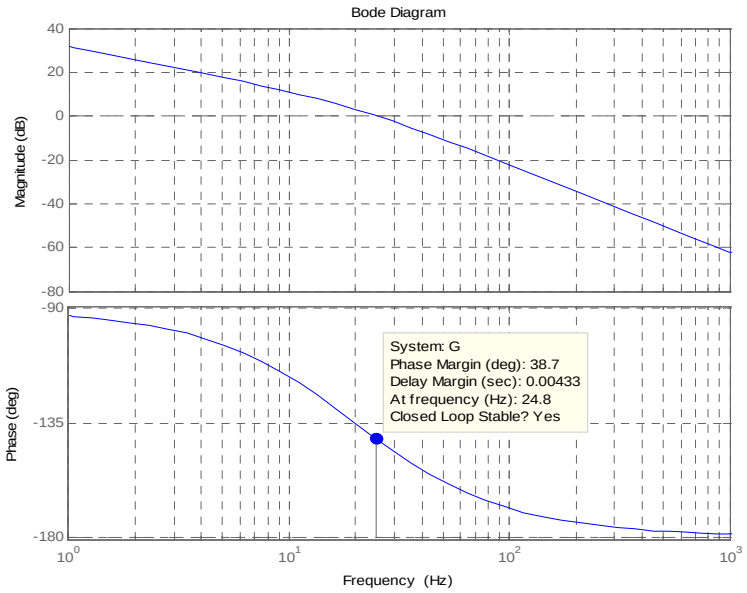

Fig. 3.3 The Bode plots of the PLL.

3.2 DC-AC Conversion

To achieve the bi-directional power flow feature of the MSBG-inverter, two main operation modes of the BBCs will be discussed. For dc-ac conversion of the first BBC set in Fig. 3.1, Fig. 3.4 and Fig. 3.5 show the two-sub-operating modes in the positive half cycle and negative cycle of the grid. When S_{d1} operates, the current i_{L1} is increased because the voltage across inductor L_1 is positive. When S_{d1} is turned off,

doi:10.6342/NTU201603394

the current i_{L1} is decreased and the energy of L_1 is transferred to the ac mains.

For dc-ac conversion of the first BBC set in Fig. 3.1, the switch S_{c1} is always turned off and the gate signal of S_{d1} can be generated by comparing the rectified sinusoidal signal V_{sin} which can be obtained via the PLL with the saw-tooth carrier signal V_{saw} in discontinuous current mode (DCM) operation as shown in Fig. 3.6(a). Also, the switch S_{c1} is turned-on naturally in zero current switching (ZCS) due to the operation in DCM. In addition, a natural PFC function and the simplified EMI filter design are maintained in the proposed MSG-inverter.

Because of the rectified SPWM control with DCM operation, the waveform of the inductor current, i_{L1}, has an envelope of the rectified ac mains. During the half-cycle of the grid line, the total switching numbers N can be expressed as:

$$N = \frac{f_s}{2f} \tag{3.5}$$

where f_s is the switching frequency and f is the grid frequency. Typical waveforms of the inductor current, i_{L1}, and output current, i_{o1}, for the DCM operation during the k-th switching cycle are shown in Fig. 3.6(b).

In Fig. 3.6(b), $d_{d1}[k]$ and $d_{d2}[k]$ are defined as the charging duty ratio and the discharging duty ratio of the k-th switching period T_s, respectively. For the first BBC, during the charging period, the active switch S_{d1} is turned on and the voltage potential across the input inductor L_1 is equal to the input voltage V_{v1} which results in the linearly increased inductor current. When the switch S_{d1} is turned off, the voltage potential across the input inductor L_1 is reversed and equal to the capacitor voltage V_{cf} which can be assumed to be the rectified ac mains because of the unfolder.

doi:10.6342/NTU201603394

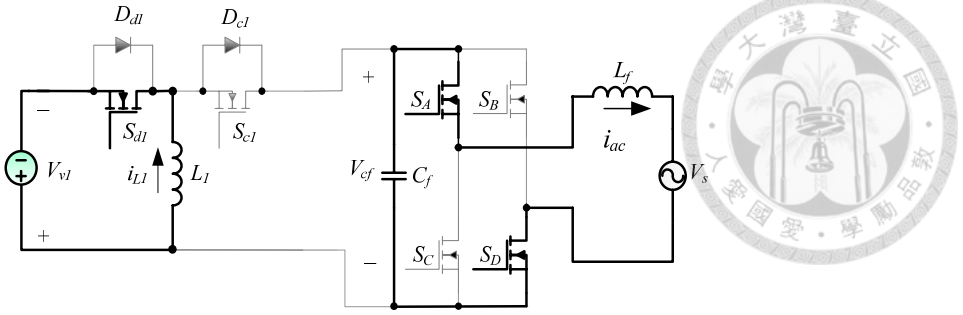

(a) S_{d1} is on

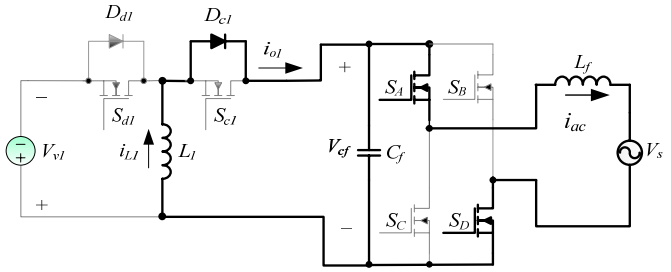

(b) S_{d1} is off

Fig. 3.4 Sub-operating modes in the positive half cycle (a) S_{d1} is on. (b) S_{d1} is off.

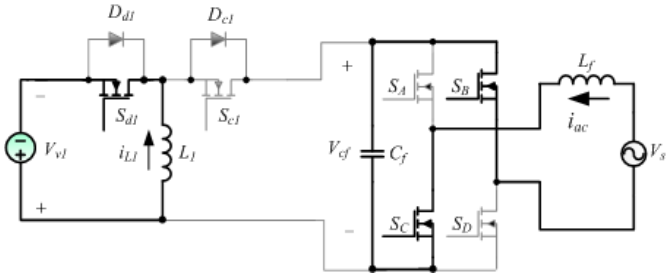

(a) S_{d1} is on

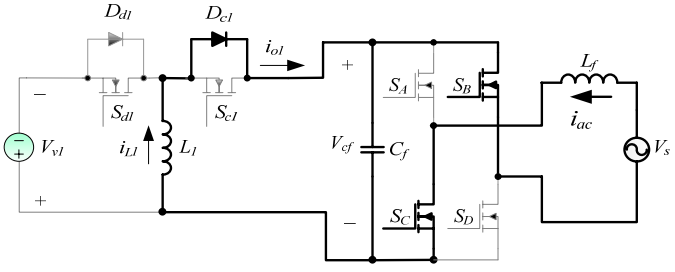

(b) S_{d1} is off

Fig. 3.5 Sub-operating modes in the negative half cycle (a) S_{d1} is on. (b) S_{d1} is off.

doi:10.6342/NTU201603394

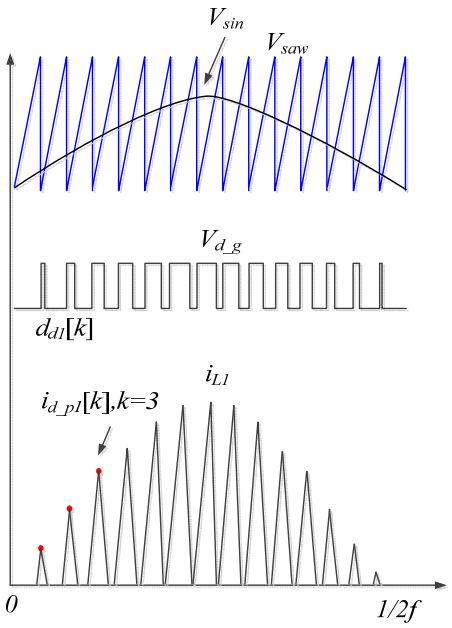

(a) The control signal generation.

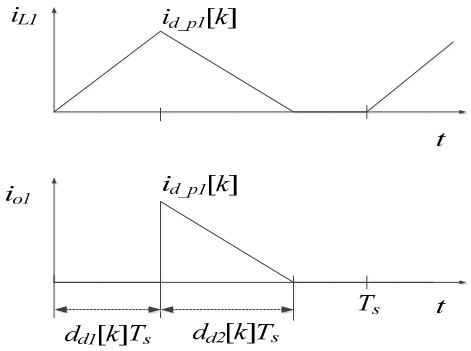

(b) Typical input inductor current and output current waveforms of the first BBC during the *k*-th switching cycle in DC-AC conversion mode.

Fig. 3.6 The control signal generation and input inductor current waveform of the first BBC in DC-AC conversion mode.

Due to the DCM operation, the inductor current i_{L1} decreases to zero during the discharging period. The peak current of the input inductor of the *k*-th switching cycle can be expressed as:

$$i_{d\_p1}[k] = \frac{V_{v1}}{L_1} \cdot d_{d1}[k]T_s = \frac{V_{cf}[k]}{L_1} \cdot d_{d2}[k]T_s \qquad (3.6)$$

where $V_{cf}[k]$ is the output capacitor voltage during the *k*-th switching cycle. Due to the DCM SPWM control, (3.6) can be further modified as:

doi:10.6342/NTU201603394

$$i_{d\_p1}[k] = \frac{V_{v1}}{L_1 f_s} \cdot D_{p1} \sin(\frac{k\pi}{N}) \tag{3.7}$$

where D_{p1} is the maximum duty ratio during the half-cycle of the grid line. To ensure the DCM operation in DC-AC conversion mode, the charging current must be smaller than the discharging current of the input inductor and follow the restriction:

$$V_{v1} \frac{D_{p1} T_s}{L_1} < \sqrt{2} V_{ac} \frac{(1 - D_{p1}) T_s}{L_1} . \tag{3.8}$$

Thus, the restriction can be rewritten as:

$$D_{p1} < (\frac{\sqrt{2} V_{ac}}{V_{v1} + \sqrt{2} V_{ac}}) \tag{3.9}$$

where V_{ac} is the rms value of utility grid line voltage. It should be mentioned that the desired D_{p1} can be easily obtained by controlling the amplitude of the rectified sinusoidal signal V_{sin} as shown in Fig. 3.3(a).

The average output current of the first BBC during the positive half-cycle can be derived as:

$$< i_{o1} > = \frac{1}{N} \sum_{k=1}^{N} \frac{i_{d\_p1}[k] d_{d2}[k] T_s}{2} \tag{3.10}$$

From (3.6) and (3.10), the average value of the output impedance of BBC can be expressed as follows:

$$\frac{< V_{cf} >}{< i_{o1} >} = \frac{1}{N} \sum_{k=1}^{N} \frac{2 L_1 V_{cf}^{\ 2}[k]}{V_{v1}^{\ 2} d_{d1}^{\ 2}[k] T_s^{\ 2}} \tag{3.11}$$

In (3.11), the ratio of V_{cf} and d_{d1} for each k-th switching cycle can be approximated as a constant since both of them can be approximated as rectified sinusoidal functions. It implies that the BBC has a constant output impedance and can inject power into the ac mains with an almost unity power factor. On the order hand, the proposed MSBG-inverter cannot provide the ac mains with reactive power.

doi:10.6342/NTU201603394

Due to the DCM SPWM control with the current waveforms shown in Fig. 3.6(b), the average DC-AC input power can be obtained as:

$$P_{i1} = \frac{V_{v1}}{2N}\sum_{k=1}^{N} i_{d\_p1}[k]d_{d1}[k] \tag{3.12}$$

Combining (3.6), (3.7), and (3.13), the expression of the average DC-AC input power becomes:

$$P_{i1} = \frac{f}{L_1 f_s^2}\sum_{k=1}^{N}\left(V_{v1}D_{p1}\cdot\sin(\frac{k\pi}{N})\right)^2 \tag{3.13}$$

Eq. (3.13) reveals that the average DC-AC input power is only related to V_{v1} and D_{p1} if other parameters (f, f_s, N, and L_1) are carefully designed. In other words, the input power of the BBC can be determined without measuring the DC current. By measuring the voltage source V_{v1} to generate appropriate maximum duty ratio D_{p1} of the BBC, it is possible to realize the individual power-handling capability required for multi-input grid-connected inverter system.

3.3 AC-DC Conversion

For ac-dc conversion of the first BBC set in Fig. 3.1, Fig. 3.7 and Fig. 3.8 show the two-sub-operating modes in the positive half cycle and negative cycle of the grid, respectively. When S_{c1} operates, the current i_{L1} is decreased because the voltage across inductor L_1 is negative. When S_{c1} is turned off, the current i_{L1} is increased and the energy of L_1 is transferred to the voltage source. For AC-DC conversion mode, the switch S_{d1} is always turned off and the gate signal of S_{c1} can be generated by comparing the reference signal V_{ref} with the saw-tooth carrier signal V_{saw} with DCM operation as shown in Fig. 3.9(a). In Fig. 3.9(b), d_{c1} is defined as the charging duty ratio and $d_{c2}[k]$ is defined as the discharging duty ratio of the k-th switching period T_s,

doi:10.6342/NTU201603394

respectively. For the first BBC, during the charging period, the active switch S_{c1} is turned on and the voltage potential across the input inductor L_1 is equal to the capacitor voltage V_{cf} which can be assumed to be the rectified ac mains because of the unfolder. When the switch S_{c1} is turned off, the voltage potential across the input inductor L_1 is reversed and equal to the voltage source V_{v1} which results in the linearly decreased inductor current. Due to the DCM operation, the inductor current i_{L1} decreases to zero during the discharging period. The peak current of the input inductor of the k-th switching cycle can be expressed as:

$$i_{c\_p1}[k]=\frac{V_{cf}[k]}{L_1}\cdot d_{c1}T_s=\frac{V_{v1}}{L_1}\cdot d_{c2}[k]T_s \tag{3.14}$$

Also, to ensure the DCM operation in AC-DC conversion mode, the charging current must be smaller than the discharging current of the input inductor and follow the restriction:

$$\sqrt{2}V_{ac}\frac{d_{c1}T_s}{L_1}<V_{v1}\frac{(1-d_{c1})T_s}{L_1}. \tag{3.15}$$

Thus, the restriction can be rewritten as:

$$d_{c1}<\left(\frac{V_{v1}}{V_{v1}+\sqrt{2}V_{ac}}\right) \tag{3.16}$$

Due to the DCM SPWM control with the current waveforms shown in Fig. 3.4(b), the average AC-DC output power can be obtained as:

$$P_{i1}=\frac{f{d_{c1}}^2}{L_1{f_s}^2}\sum_{k=1}^{N}\left(V_{cf}[k]\right)^2 \tag{3.17}$$

Eq. (3.17) reveals that the average AC-DC output power is only related to $V_{cf}[k]$ and d_{c1} if other parameters (f_s, N, and L_1) are carefully designed. Also, the AC-DC output power can be determined without measuring the DC current.

doi:10.6342/NTU201603394

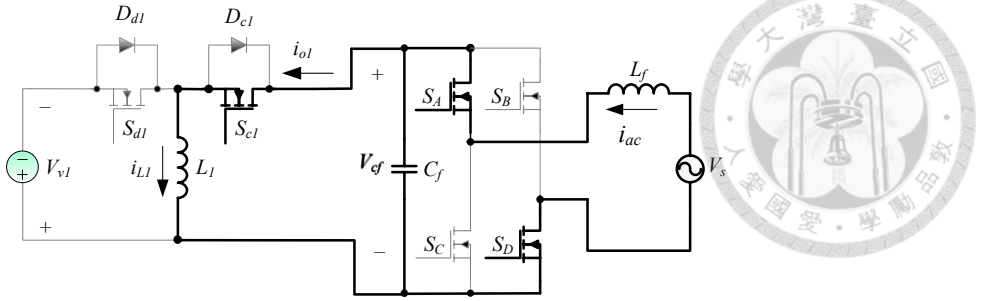

(a) S_{c1} is on

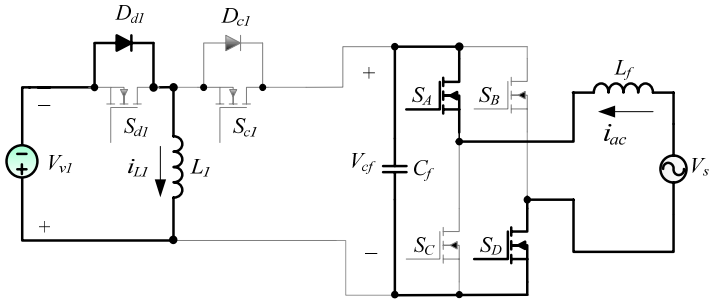

(b) S_{c1} is off

Fig. 3.7 Sub-operating modes in the positive half cycle (a) S_{c1} is on. (b) S_{c1} is off.

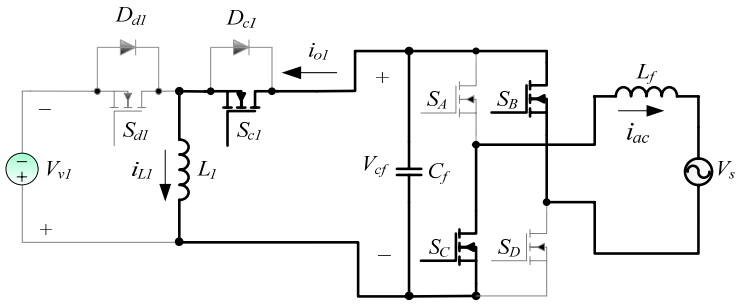

(a) S_{c1} is on.

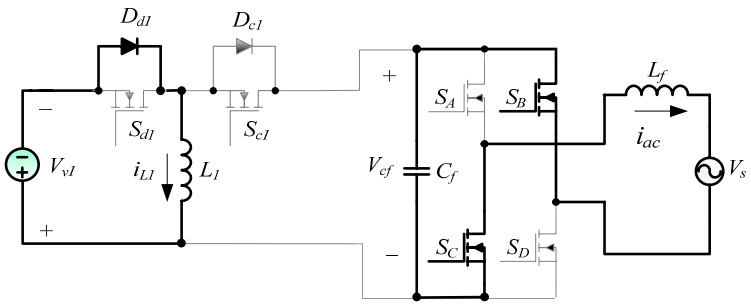

(b) S_{c1} is off.

Fig. 3.8 Sub-operating modes in the negative half cycle (a) S_{c1} is on. (b) S_{c1} is off.

doi:10.6342/NTU201603394

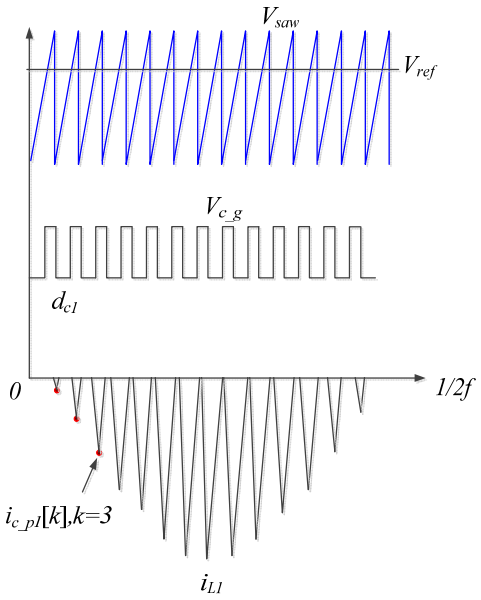

(a) The control signal generation.

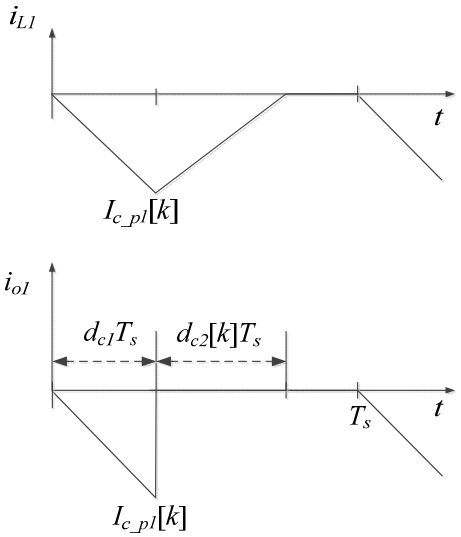

(b) Typical input inductor current and output current waveforms of the first BBC during the *k*-th switching cycle in AC-DC conversion mode.

Fig. 3.9 The control signal generation and input inductor current waveform of the first BBC in AC-DC conversion mode.

3.4 Interleaving Operation

For the proposed MSBG-inverter, the m-sets of BBCs can operate in the interleaving fashion. The required synchronization signal for the interleaving operation can be easily obtained from the ac line voltage and no extra communication

doi:10.6342/NTU201603394

between BBC is required. By shifting the duty cycles of adjacent channels with 360^o/m, the total current ripple of the output inductor can be greatly reduced. Fig. 3.10 shows the voltage and current waveforms of the BBC's output of two phase interleaving in DC-AC conversion mode. The shifting time T_m of m-sets of BBCs can be expresses as:

$$T_m = \frac{1}{mf_s} \tag{3.18}$$

Since the average voltage of output inductor L_f is zero at steady state, the average voltage across C_f is equal to V_{ac} and the peak discharging time T_{off} can be expressed as:

$$T_{off} = \frac{V_{v1}D_{p1}}{\sqrt{2}V_{ac}f_s} \tag{3.19}$$

The discharging time of the capacitor C_f can be expressed as:

$$T_d = T_m - T_{off} = \frac{1}{mf_s} - \frac{V_{v1}D_{p1}}{\sqrt{2}V_s f_s} \tag{3.20}$$

The peak deviation of the output capacitor can be derived as:

$$\Delta V_{C_f} = \frac{T_d I_{ac}}{C_f} \tag{3.21}$$

where C_f is the capacitor value and I_{ac} is the peak value of the output current. Since the variation of the storage energy of the output capacitor is almost equal to the variation of the storage energy of the output inductor in T_m interval, the equation for the storage energy can be derived as:

$$E_d = \frac{1}{2}C_f \Delta V_{C_f}{}^2 = \frac{1}{2}L_f \Delta I_f{}^2 \tag{3.22}$$

where L_f is the output inductor value and ΔI_f is the peak current deviation of the output inductor. From (3.20), (3.21), (3.22), and Fig. 3.5, the peak current deviation of

doi:10.6342/NTU201603394

the output inductor can be obtained as:

$$\Delta I_f = \sqrt{\frac{\left(\frac{1}{mf_s} - \frac{V_{b1}D_{p1}}{\sqrt{2}V_s f_s}\right)^2 I_{ac}^{\ 2}}{L_f C_f}} \tag{3.23}$$

From (3.23), it can be founded that the ripple current can be decreased by adding the numbers of the BBCs directly.

On the other hand, Fig. 3.11 shows the voltage and current waveforms of the BBC's output of two phases interleaving in AC-DC conversion mode. The average voltage across C_f is equal to V_{ac} and the charging time T_{on} can be expressed as:

$$T_{on} = \frac{d_{c1}}{f_s} \tag{3.24}$$

The charging time of the capacitor C_f can be expressed as:

$$T_c = T_m - T_{on} = \frac{1}{mf_s} - \frac{d_{c1}}{f_s} \tag{3.25}$$

The peak deviation of the output capacitor can be derived as:

$$\Delta V_{C_f} = \frac{T_c I_{ac}}{C_f} \tag{3.26}$$

From (3.24), (3.25), (3.26), and Fig. 3.6, the peak current deviation of the output inductor can be obtained as:

$$\Delta I_f = \sqrt{\frac{\left(\frac{1}{mf_s} - \frac{d_{c1}}{f_s}\right)^2 I_{ac}^{\ 2}}{L_f C_f}} \tag{3.27}$$

From (3.23) and (3.27), it can be founded that the ripple current can be decreased by adding the numbers of the BBCs directly. This interleaved operation can achieve not only the higher ripple frequency of the output current that the size of the output inductor and capacitor can be reduced but also the ripple current reduction because of the gap or overlap in different current phase of each BBC. Moreover, the interleaving

doi:10.6342/NTU201603394

operation increases the switching frequency without increasing the switching losses. The obvious benefit is an increase in the power density without the penalty of reduced power-conversion efficiency.

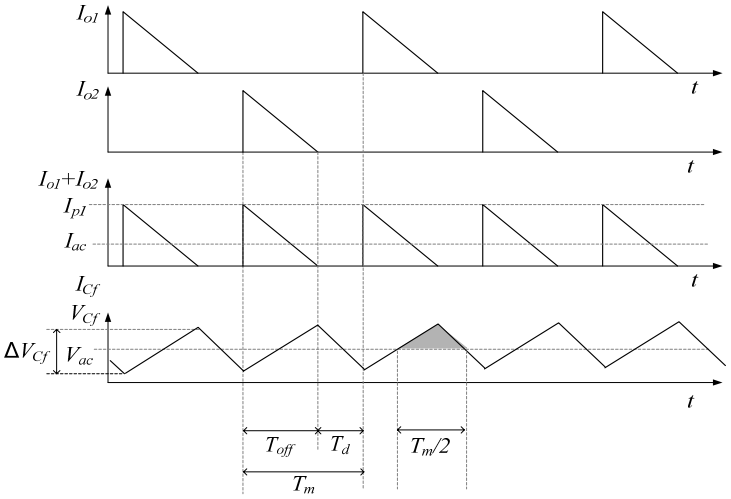

Fig. 3.10 The output voltage and current waveforms of the BBC of two phase interleaving in DC-AC conversion mode.

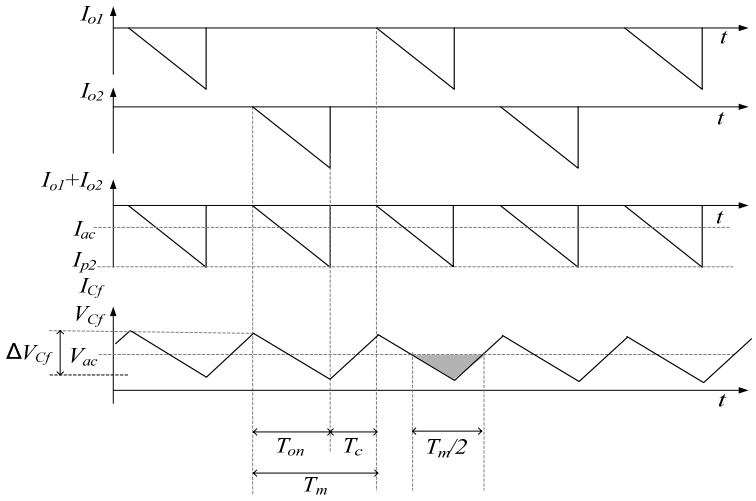

Fig. 3.11 The output voltage and current waveforms of the BBC of two phase interleaving in AC-DC conversion mode.

doi:10.6342/NTU201603394

3.5 Loss Consideration

The proposed MSBG-inverter can be classified as a single-stage converter since the unfolder only operates at the zero-crossing of the line voltage and its switching loss can be neglected. Major losses of the BBC come from device conduction, switching and inductor. Form (3.7) and (3.14), the rms current of S_{d1} and S_{c1} of the k-th switching cycle can be expressed as:

$$i_{d1(k)} = \sqrt{\frac{1}{3}\left(D_{p1}\sin(\frac{k\pi}{N})\right)^2\left(\frac{V_{v1}}{L_1 f_s}\right)} \tag{3.28}$$

$$i_{c1(k)} = \sqrt{\frac{1}{3}d_{c1}{}^2\left(\frac{V_{cf[k]}}{L_1 f_s}\right)} \tag{3.29}$$

For the first BBC set, the conduction losses of the S_{d1} and S_{c1} can be estimated by:

$$P_{d1(cond)} = \frac{R_{d1\_ds(ON)}}{3N}\sum_{k=1}^{N}\left(D_{p1}\sin(\frac{k\pi}{N})\right)^2\left(\frac{V_{b1}}{L_1 f}\right)^2 \tag{3.30}$$

$$P_{c1(cond)} = \frac{d_{c1}R_{c1\_ds(ON)}}{3N}\sum_{k=1}^{N}\left(\frac{V_{cf}[k]}{L_1 f}\right)^2 \tag{3.31}$$

where $R_{d1\_ds(ON)}$ and $R_{c1\_ds(ON)}$ are the turn-on resistance of S_{d1} and S_{c1}, respectively. With the DCM operation, the switches S_{d1} and S_{c1} are turned-on at zero current and nearly lossless. For the turn-off transient, the switch current of S_{d1} and S_{c1} fall to zero and the worst case value of the current fall-time can be read from the switch data-sheet. The turn-off current of S_{d1} and S_{c1} of the k-th switching cycle can be obtained from (3.7) and (3.14). Therefore, the turn-on switching losses of S_{d1} and S_{c1} can be neglected. For example, the key components S_{d1} and S_{c1} are both used by MOSFET and The turn-off loss of S_{c1} and S_{d1} can be approximated by [43]:

doi:10.6342/NTU201603394

$$P_{d1(\text{turn-off})} = \frac{T_{off}}{2N}\sum_{k=1}^{N}\left[\frac{V_{b1}}{L_1}\cdot D_{p1}\sin(\frac{k\pi}{N})\cdot\left(V_{v1}+\sqrt{2}V_{ac}\sin(\frac{k\pi}{N})\right)\right] \quad (3.32)$$

$$P_{c1(\text{turn-off})} = \frac{T_{off}}{2N}\sum_{k=1}^{N}\left[\frac{\sqrt{2}V_{ac}}{L_1}\cdot d_{c1}\sin(\frac{k\pi}{N})\cdot\left(V_{v1}+\sqrt{2}V_{ac}\sin(\frac{k\pi}{N})\right)\right] \quad (3.33)$$

where T_{off} is the turn-off transient time which is a function of the driving current and the input capacitor C_{iss} of the datasheet. In addition to the switching loss, the C_{oss} loss is minor and the C_{oss} loss can be calculated as:

$$P_{\text{coss(Sd1)}} = \frac{1}{2}C_{oss(Sd1)}\cdot V_{d1\_DS(turn-on)}{}^{2}\cdot f_{sw} \quad (3.34)$$

$$P_{\text{coss(Sc1)}} = \frac{1}{2}C_{oss(Sc1)}\cdot V_{c1\_DS(turn-on)}{}^{2}\cdot f_{sw} \quad (3.35)$$

where $C_{oss(Sd1)}$ and $C_{oss(Sc1)}$ are the equivalent drain-to-source capacitance, $V_{d1\_DS(turn-on)}$ and $V_{c1\_DS(turn-on)}$ are the drain-to-source turn-on voltage for S_{d1} of and S_{c1}. The inductor loss can be calculated as:

$$P_{L_1} = P_{copper} + P_{core} \quad (3.36)$$

where P_{copper} and P_{core} are the copper-loss and core-loss of the inductor. The copper-loss is easily obtained by multiplying the square value of the inductor rms current by the ESR of L_1. The core-loss generated by changing magnetic flux field within the material is a function of half of the AC flux swing and frequency ant it can be approximated as:

$$P_{core} = aB_{pk}{}^{b}f^{c} \quad (3.37)$$

where a, b, c are constants determined from curve fitting in the core data-sheet, and B_{pk} is defined as half of the AC flux swing. As a result, the frequency should be selected by compromising between switching loss, core loss and copper loss. Moreover, the C_f loss and unfolder loss are also significant and the C_f loss can be calculated as:

doi:10.6342/NTU201603394

$$P_{Cf} = I_{Cf}^{\ 2} \cdot R_{Cf} \tag{3.38}$$

where I_{Cf} is the rms value of the C_f current and R_{Cf} is the ESR of C_f. The unfolder loss is the conduction loss of the 4 switches that can be calculated as:

$$P_{Unfolder} = 2 \cdot I_o^{\ 2} \cdot R_{A\_ds(ON)} \tag{3.39}$$

where $R_{A\_ds(ON)}$ are the turn-on resistance of S_A.

The total loss of the proposed MSBG-inverter in dc-ac conversion mode can be expressed as:

$$P_{Total\,(DC-AC)} = P_{D1(comduction)} + P_{D1(turn-off)} + P_{Coss\,(S_{D1})} + P_{L_1} + P_{C_f} + P_{Unfolder} \tag{3.40}$$

The total loss of the proposed MSBG-inverter in ac-dc conversion mode can be expressed as:

$$P_{Total\,(DC-AC)} = P_{C1(comduction)} + P_{C1(turn-off)} + P_{Coss\,(S_{C1})} + P_{L_1} + P_{C_f} + P_{Unfolder} \tag{3.41}$$

3.6 Summary

In this dissertation, an MSBG-inverter without using current sensors is proposed. The rectified sinusoidal envelop-shaped pulsating output current of the BBC is injected into the ac mains via the unfolder, which consists of 4 active switches and a LC filter. Since the unfolder is switched at the ac line frequency, its switching loss is very low and can be neglected. Therefore, the proposed MSBG-inverter only has one high-frequency PWM signal and can be categorized as a single-stage inverter. If the low conduction voltage drop power MOSFET and ultra-fast reverse recovery diode are used, the proposed MSBG-inverter can be very efficient. Finally, the design procedure of the proposed MSBG-inverter can be summarized as follows:

1) To ensure the DCM operation of the BBC, determine an eligible maximum duty

doi:10.6342/NTU201603394

ratio shown in (3.9) and (3.16) according to the rated voltage of the dc voltage source and the ac-mains.

2) Select the appropriate switching frequency and determine the total switching numbers shown in (3.5) with grid frequency.

3) Design the input inductor L_1 shown in (3.13) and (3.17) with the circuit parameters f, fs, D_{p1}, d_{c1}, N, and P_{b1}.

4) Based on the numbers of voltage sources, shift the duty cycles of adjacent channels with 360^{o}/m for the interleaving operation.

5) Select the appropriate value of the output current ripple to determine the output inductor and capacitor shown in (3.23) and (3.27) with the circuit parameters m, T_m, L_{p1}, L_1, V_s, and I_{ac}.

doi:10.6342/NTU201603394

Chapter 4 The MSBG Inverter for PV System Applications

Fig. 4.1 shows the block diagram of a conventional PV system with MPPT function. The roles of the dc-dc converter and dc-ac inverter are to transfer the DC power into AC power and optimize the harvest power of the PV panels under different irradiance with MPPT function. However, the control current is relatively complex and the two-stages configuration is needed while cost will be increased because of the requirement of the additional sensing circuit. The proposed MSBG-inverter is one of the ways to realize the DMPPT function and improve the above drawbacks. For the grid-connected PV system application, Each PV panel has its own dc-dc converter to fulfill the MPPT feature while the unfolder is realized by an output inductor and four active switches operated at ac line frequency. The dc-dc converter produces a high frequency pulsating dc current with a rectified sinusoidal envelope. The MPPT feature can be achieved by adjusting the maximum duty of the power switch in the dc-ac converter. The unfolder can convert the high frequency pulsating dc current generated by the dc-dc converters into a sinusoidal one with utility line frequency.

4.1 PV Panel

Fig. 4.2 shows a common electrical model of PV panel including the shunt resistor R_{SH} that controls the leakage current. The PV current can be expressed as:

$$I_{PV} = I_{SC} - I_S(e^{\frac{V}{nV_T}} - 1) - \frac{V}{R_{SH}} \tag{4.1}$$

where I_{sc} is the short circuit current, I_s is the diode reverse current, n is diode ideality factor, and V_T is the temperature voltage. Based on the electrical model of PV panel, the nonlinear I-V characteristic curve can be obtained. Fig. 4.3 shows the I-V

doi:10.6342/NTU201603394

characteristic curve of a commercial product [44]. It can be observed that the I-V curve highly depends on the irradiance. Therefore, MPPT function is required to extract the maximum power from the PV array under different irradiance conditions.

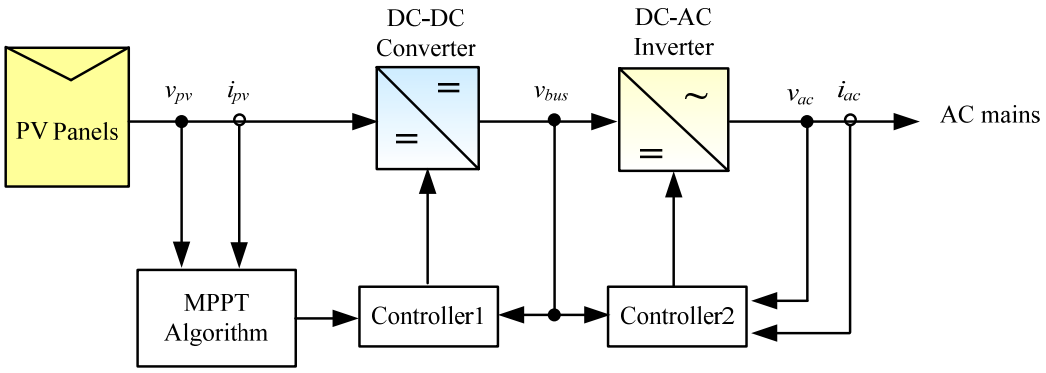

Fig. 4.1 Block diagram of a conventional PV system with MPPT function.

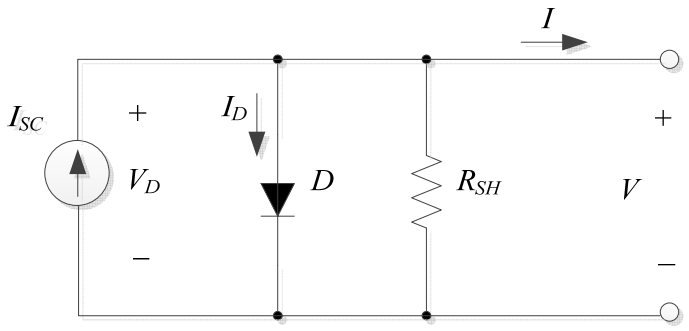

Fig. 4.2 The electrical model of the PV panel.

doi:10.6342/NTU201603394

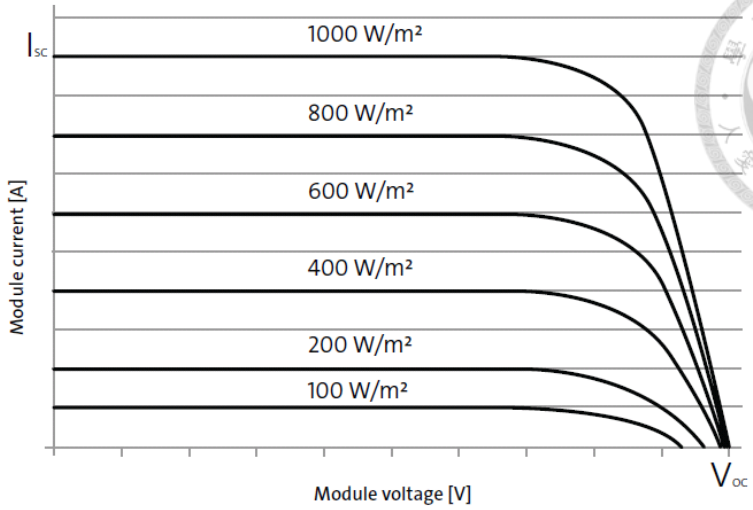

Fig. 4.3 The I-V characteristic curve of a commercial product.

4.2 DMPPT

Usually, a PV power system consists of many PV panels arranged in strings by series or parallel connections. The output power of a PV panel always depends on its operating voltage, the irradiance, and the temperature. The non-uniform insulation could easily reduce the total output power of the PV power system. For example, a PV power system formed by two-series-connected PV panels with partial shading is shown in Fig. 4.4(a). Its corresponding I-V and P-V curves are shown in Fig. 4.4(b) where the extra local maximum power point may trap the MPPT controller. Even through the global maximum power point is found, the total output power of the two PV panels is still not the actual maximum power obtained from the two individual PV panels. One way to solve this problem is to use the DMPPT method. In general, the main disadvantage of the DMPPT PV system in comparison to the central MPPT PV system is the need of many power converters, which increase the installation cost and reduce the power conversion efficiency. Also, expensive current sensors are required to calculate the PV output power for maximum power tracking. Both the two-stage

doi:10.6342/NTU201603394

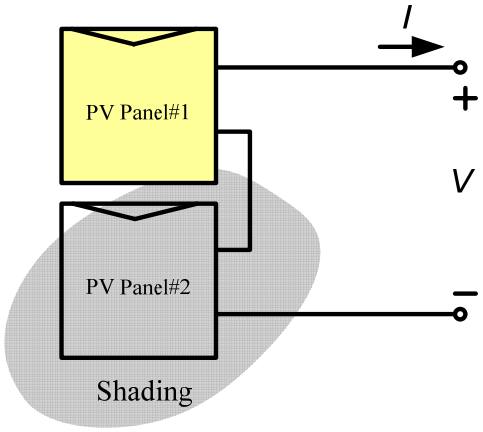

(a)

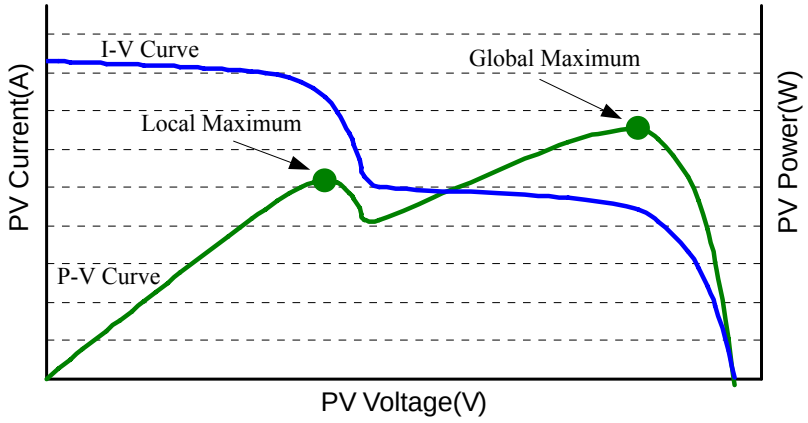

(b)

Fig. 4.4 Two-series-connected PV panels with partial shading (a) Two series-connected PV panel. (b) The corresponding I-V and P-V curve with partial shading.

configuration and the expensive current sensor both become the major disadvantages for the DMPPT PV system. Therefore, the proposed MSBG-inverter is one of the ways to solve the above problems.

Because of the nonlinear voltage-current characteristic of the PV panel, the perturbation and observation (P&O) strategy is commonly used to achieve the MPPT function because of its simplicity. For the conventional P&O MPPT control, the input

doi:10.6342/NTU201603394

current information is always needed to calculate the PV power. For the proposed MSBG-inverter, the input power can be easily determined and controlled without using expensive current sensors.

The flowchart of the P&O MPPT algorithm for the proposed MSBG-inverter is shown in Fig. 4.5. The interrupt period is a user defined parameter which ranges from 10 to 100 ac cycles. At the beginning of the interrupt routine, the present input power P_{L1} supplied by the PV panel is calculated by using (3.10). Then, the present PV power P_{L1} is compared with the previous PV power P_{L1_old} to determine the status of the PV power. According to the PV power comparison result and the maximum duty change trend ΔD_p in the previous interrupt routine, the maximum duty ratio D_p will be either increased or decreased by modifying the amplitude of the rectified sinusoidal reference signal V_{sin} as shown in Fig. 3.6 (a). For example, if $P_{L1}>P_{L1\_old}$ and $\Delta Dp>0$, the new D_p is determined as the one in the previous interrupt routine, D_{p_old}, plus a constant quantity ΔD. On the other hand, if $P_{L1}>P_{L1\_\mathrm{old}}$ and $\Delta D_p<0$, the new D_p becomes D_{p_old}-ΔD. It should be mentioned that ΔD is a user defined parameter with the trade-off between the speed and the efficiency of the MPPT. Before exiting the interrupt routine, the present PV power and the maximum duty change trend should be saved. The P&O MPPT strategy can be easily applied to the proposed MSBG-Inverter.

doi:10.6342/NTU201603394

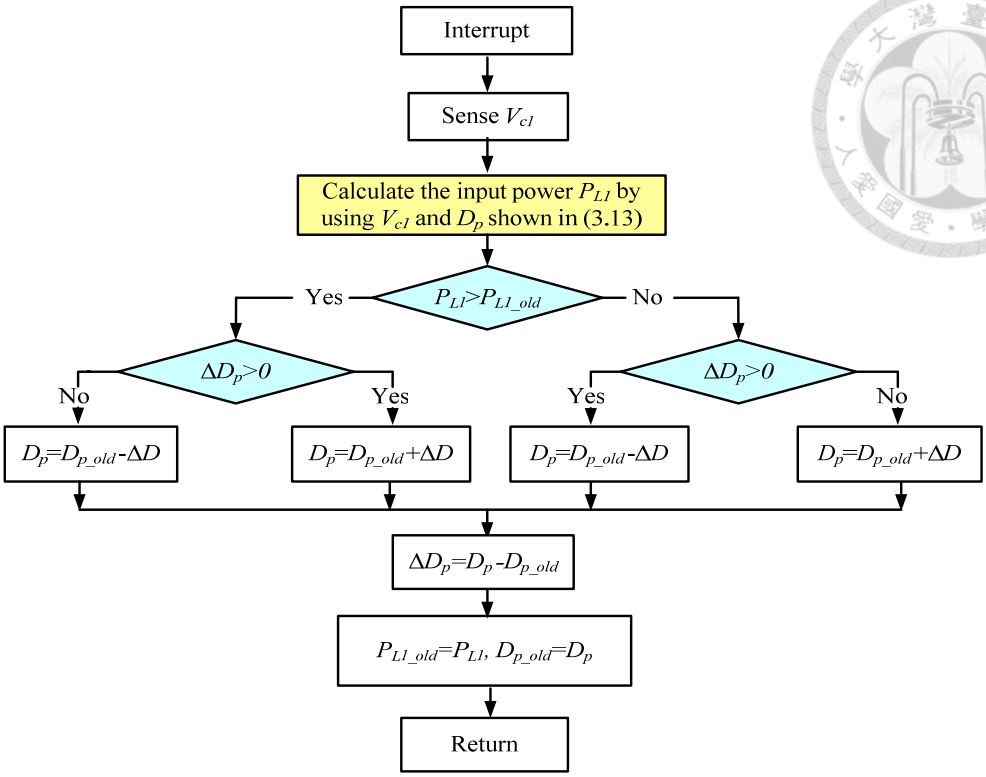

Fig. 4.5 The P&O MPPT flowchart for the proposed MSBG-inverter.

4.3 MSBG-Inverter for the PV System

Fig. 4.6 shows the proposed MSBG-inverter for the PV system application. In Fig. 4.6, by controlling the peak duty ratio and measuring V_{c1}, it is possible to obtain the input power information needed for the MPPT control strategy. Each BBC can have the distributed MPPT function and the total power is centralized to the dc-ac unfolder. Because of the nonlinear characteristics of the PV array on the power versus the voltage, the P&O is used for the MPPT function of PV systems. Generally it is necessary to calculate the PV power by the product of the voltage and the current. But in this case the peak duty cycle and V_{c1} can be used for estimating the PV power and periodically increase or decrease the duty command without using an expensive current sensor.

The control block diagram of the proposed MSBG-inverter, as an example, is

doi:10.6342/NTU201603394

shown in Fig. 4.7. The duty cycle signal, D_{p1}, can be determined by using the derived equation (3.10) without measuring the PV panel current. The synchronous rectified sinusoidal function with the grid frequency, $|sin\omega t|$, can be obtained via the PLL and is used to generate the reference signal $D_{p1}|sin\omega t|$. The gate signal of S_{d1} can be generated by comparing $D_{p1}|sin\omega t|$ with the saw-tooth carrier signal V_{saw1}.

For the PV system, the power generated from the PV panel must be kept constant for maximizing energy harvest. The MPPT provides constant output power from the PV panel, while the injected power to the grid is following a rectified sinusoidal wave. This requires energy storage elements such as capacitors to be placed between the input of the converter and the output of the PV panels for power decoupling. In Fig. 4.6 the output power of PV panel#1 without considering the conversion efficiency can be decomposed as:

$$P_{PV}(t) = I_m V_m \sin^2(2\pi ft) = \frac{1}{2} I_m V_m + \frac{1}{2} I_m V_m \cos(4\pi ft) \\ = P_{o\_av} + P_{o\_ac}(t) \tag{4.2}$$

where I_O is the peak value of i_{ac}, V_m is the peak value of v_{ac}, P_{o_av} is the output average power, which is equal to the PV output power, and $P_{o\_ac}(t)$ is the pulsating power at double-line frequency, which may get reflected into the input side, and greatly deteriorate the MPPT performance. , The decoupling capacitor value can be determined as follows [45]:

$$C_1 = \frac{P_i}{2\pi f V_{PV} \Delta V} \tag{4.3}$$

where P_i is the rated power of the PV panel, V_{PV} is the dc voltage across the decoupling capacitor C_1, and ΔV is the maximum allowable peak-to-peak voltage ripple.

doi:10.6342/NTU201603394

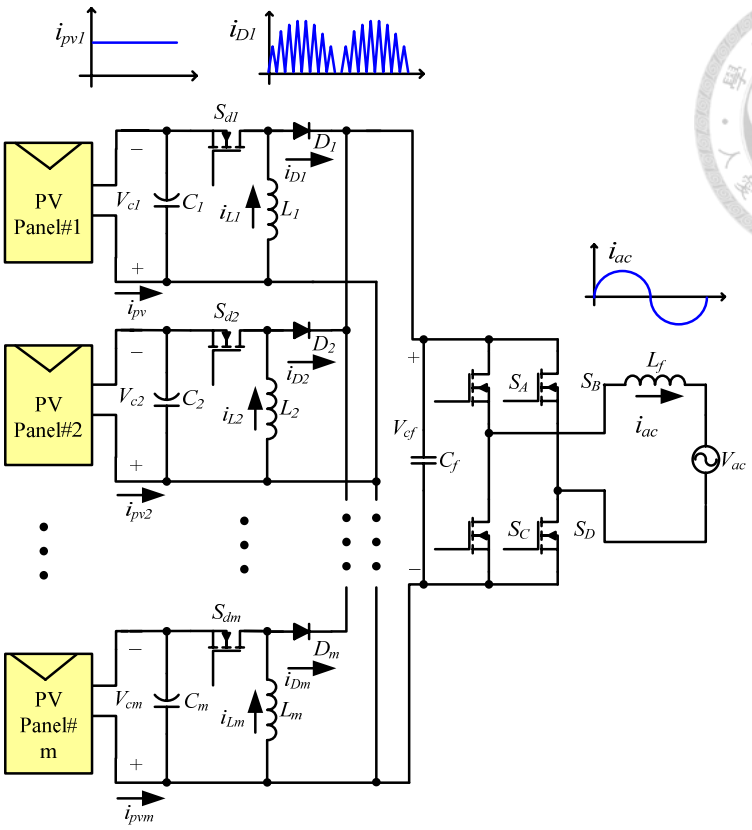

Fig. 4.6 The circuit diagram of the proposed MSBG-inverter for the PV system application

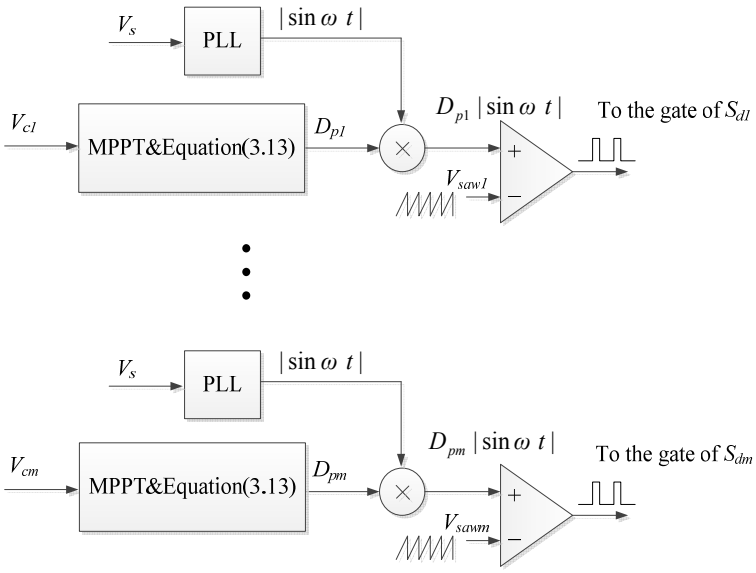

Fig. 4.7 The control block diagram of the proposed MSBG-inverter for the PV system.

doi:10.6342/NTU201603394

Table 4.1 PV panel specifications

Open circuit voltage	V_{oc} = 55 V
Short circuit current	I_{sc} = 2.5 A
MPP voltage	V_{c1} = 45 V
MPP current	I_{mp} = 2 A
MPP power	P_{L1} = 100 W

4.4 Computer Simulation and Experimental Verifications

A prototype of the proposed MSBG-inverter with two BBCs for PV system is built and tested. To achieve the desired output power, the component values and parameters must match the equations derived in previous sections. The specifications of the PV panels used for the design example are listed in Table 4.1. For the $110V_{ac,rms}$/60Hz utility line, by using (3.6), the maximum duty ratio can be obtained:

$$D_p < 0.775 \tag{4.4}$$

To achieve the same desired PV panel output power, as shown in (3.13), the input inductor L_m as a function of the switching frequency f_s. It implies that a small size inductor is possible and the weight of the proposed MSBG-inverter can be reduced. However, a high switching frequency implies a large switching loss and the trade-off between the inductance reduction and the switching loss increment need to be carefully judged. As the example shown in Fig. 4.8, there is no obvious reduction in input inductance when the switching frequency is higher than 20 kHz. Therefore, the switching frequency is selected as 20 kHz for the prototype circuit. Based on the derived mathematical equations in previous chapter, specifications of the prototype MSBG-inverter can be determined as:

1) Input inductor $L_1 = L_2$ = 120 μH

2) Input capacitor C_i = 1360 μF

doi:10.6342/NTU201603394

2) Maximum duty ratio D_p = 0.75

3) Switching frequency f_s = 20 kHz

4) Output capacitor C_f = 2μF

5) Output inductor L_f = 1.8 mH

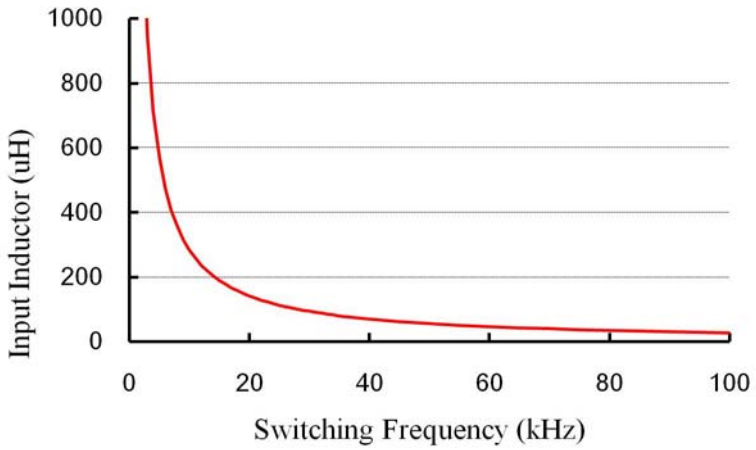

Fig. 4.8 The input inductor L_m as the function of switching frequency f_s.

With the design procedure presented in pervious chapter, the output current of the proposed MSBG-inverter can be well controlled. The computer simulation tool Simplis is used to verify the operation of the proposed MSBG-inverter for the PV system. Fig. 4.9 shows the power stage and open loop control circuit in Simplis. Fig. 4.10 shows waveforms of the gate signal V_{gs1}, input current i_{L1}, ac main voltage v_{ac}, and ac output current i_{ac}, respectively. It can be seen that the MOSFET S_{d1} is operated with ZCS at turn-on transition. In fact, all MOSFETs in each input-stage circuit of the proposed MSBG-inverter operated with ZCS at turn-on transition with similar gate signal and input current waveforms.

The simulation results shown in Fig. 4.11 are the key waveforms of the proposed MSBG-inverter with only one BBC and two interleaved BBCs operation, respectively while the output power is calculated as 100W. The MOSFET S_{d1} is operated with ZCS

doi:10.6342/NTU201603394

at turn-on transition. In Fig. 4.11, it is obvious that the input inductor current i_{Lm} has an envelope of rectified sinusoidal waveform and an almost sinusoidal output current is generated. In Fig. 4.11(a), the output current i_{ac} of the MSBG-inverter has a peak value equal to 1.5A, where the rms value of the ac mains voltage v_{ac} is 110V. In Fig. 4.11(b), the peak value of output current i_{ac} equals to 1.5A since two BBCs are interleaving. The maximum output current ripple with only one BBC operation shown in Fig. 4.11(a) is about 0.19A which is much larger than the one of 0.03A shown in Fig. 4.11(b) where two interleaved BBCs operating.

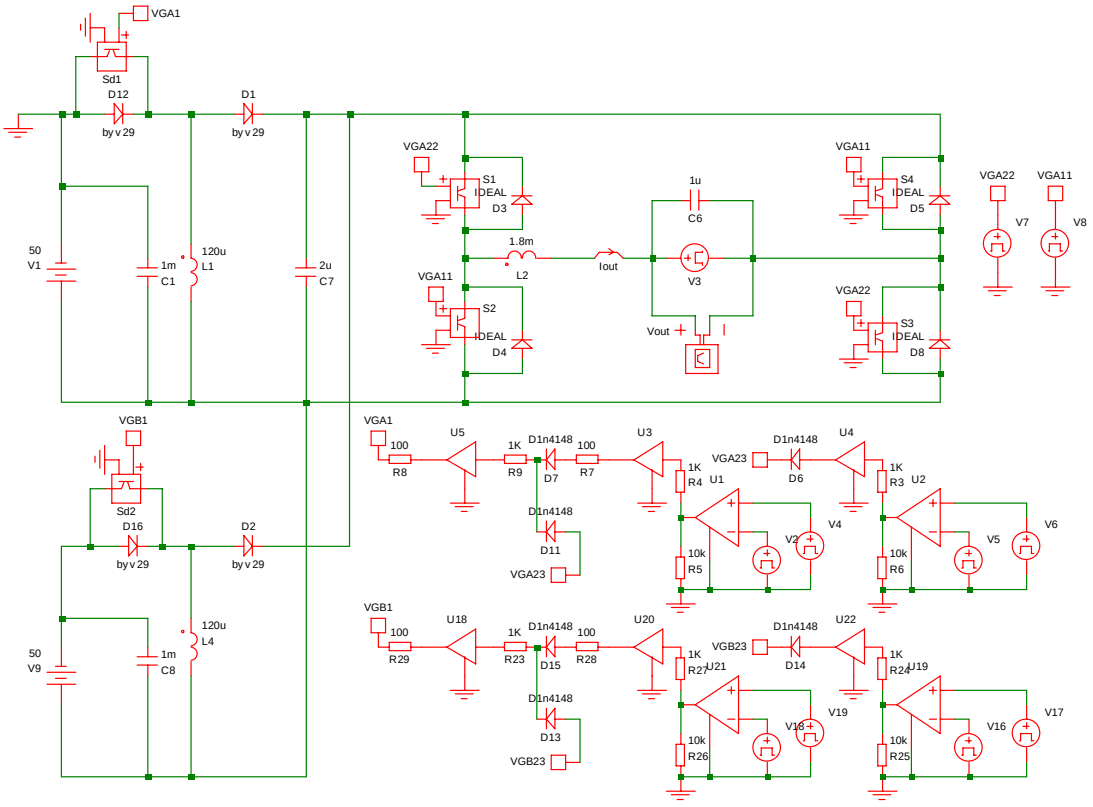

Fig. 4.9 The proposed MSBG-inverter circuit for the PV system in Simplis.

doi:10.6342/NTU201603394

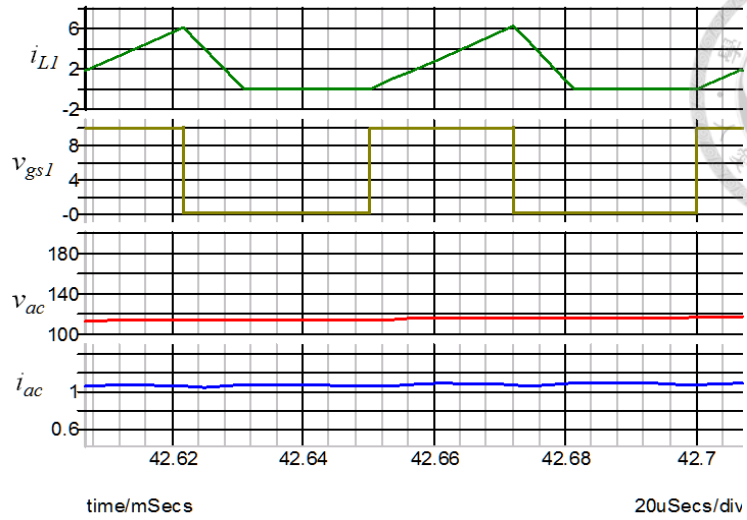

Fig. 4.10 Computer simulation of the gate signal, input current, ac main voltage, and ac output current.

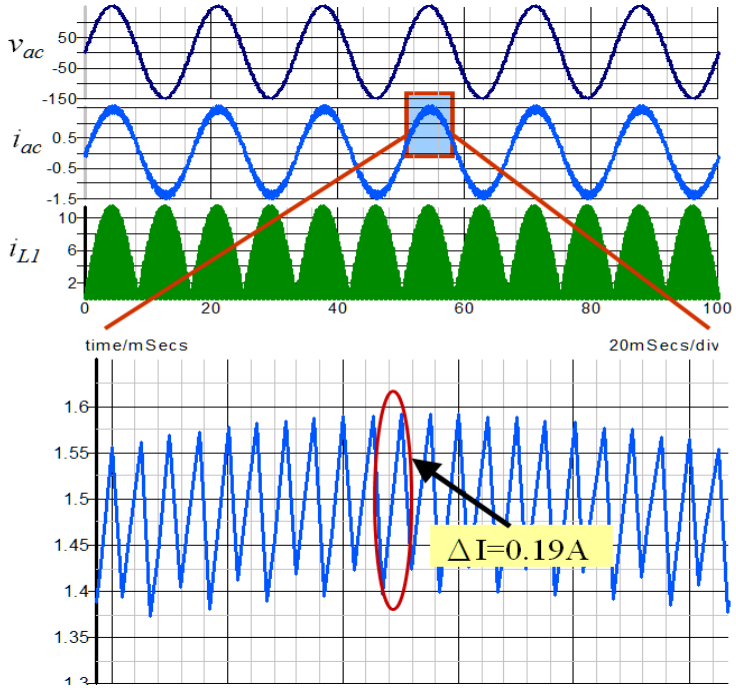

(a) non-interleaved operation

doi:10.6342/NTU201603394

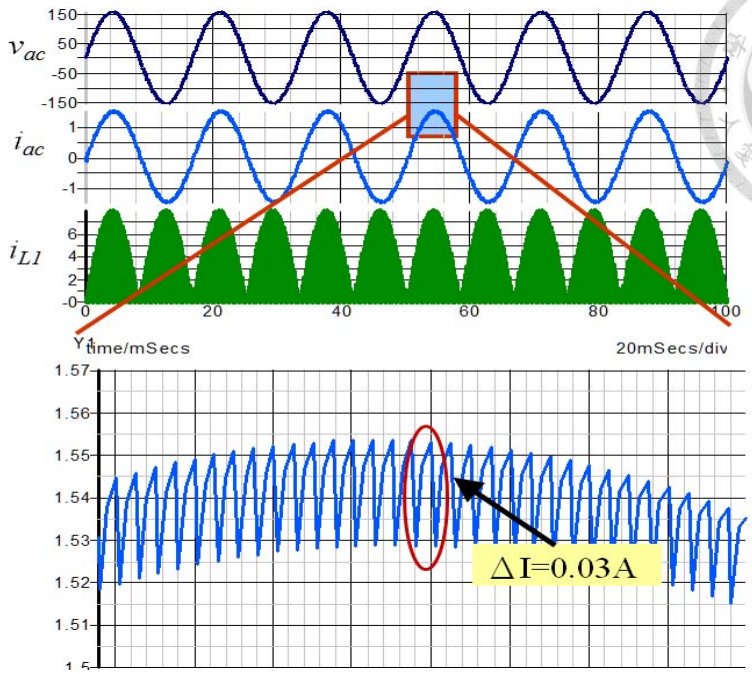

(b) interleaved operation

Fig. 4.11 Computer simulations of ac main voltage (top), ac output current (middle), and input current (bottom) for MSBG-inverter with non-interleaved or interleaved operation.

The corresponding hardware experimental waveforms of the simulated ones are shown in Fig. 4.12 and Fig. 4.13. The controller is implemented by a microprocessor, TMS320F2808, with the merit of circuit simplicity. Fig. 4.12 shows experimental waveforms and it also can be seen that the MOSFET S_{d1} is operated with ZCS at turn-on transition. In Fig. 4.13(a), the peak output current ripple with only one BBC is about 0.2A which is much larger than two interleaved BBCs operation of 0.39A in Fig. 4.13(b). Experimental waveforms are consistent with the simulated ones and the ac output current is almost in phase with the ac mains voltage.

doi:10.6342/NTU201603394

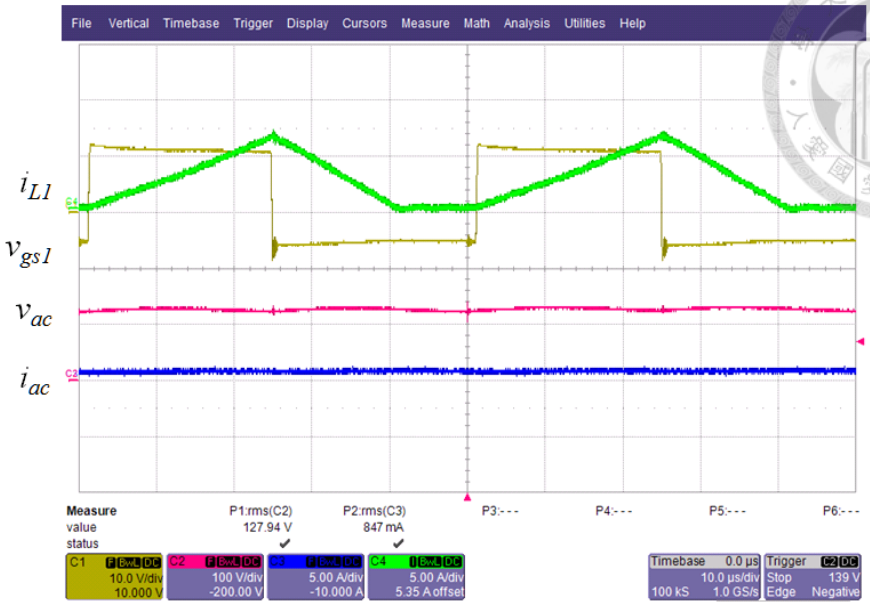

Fig. 4.12 Experimental waveforms of the gate signal, input current, ac main voltage, and ac output current.

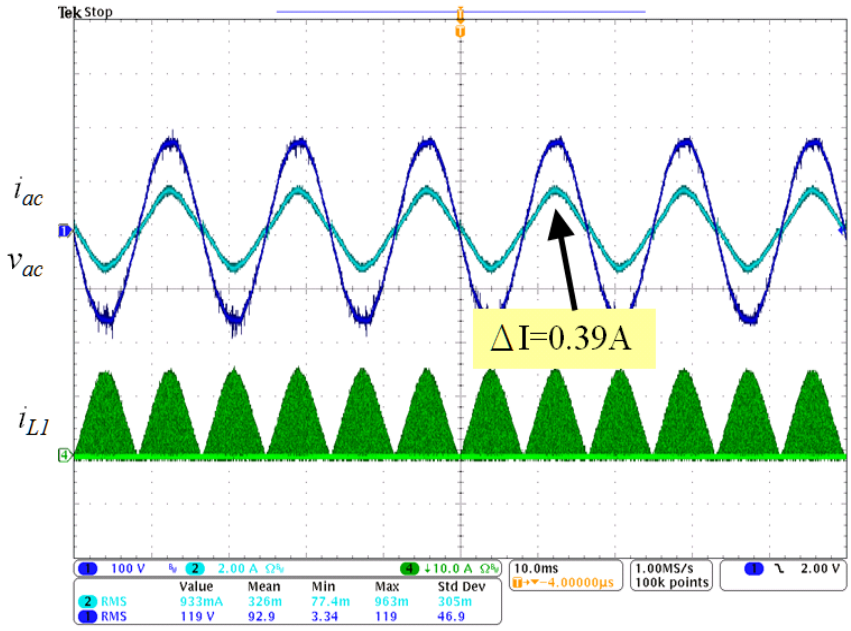

(a) non-interleaved operation

doi:10.6342/NTU201603394

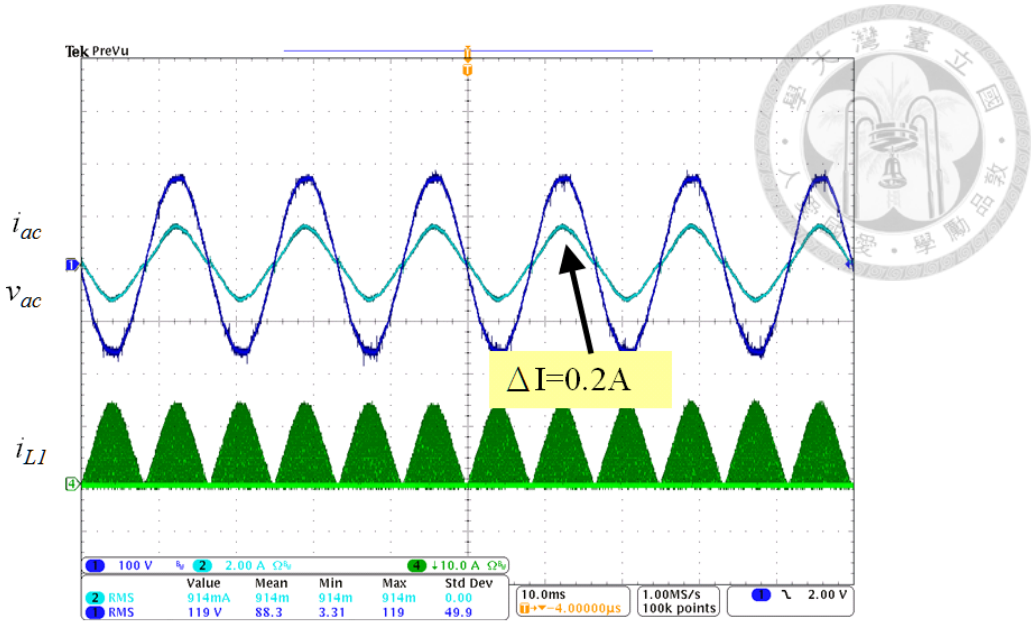

(b) interleaved operation

Fig. 4.13 Experimental waveforms of ac main voltage, ac output current, and input current for MSBG-inverter with non-interleaved or interleaved operation.

Another important feature of the MSBG-inverter is the MPPT function, where the PV simulator, Agilent E4360A, is used to simulate PV panels. Fig. 4.14 shows the MPPT efficiency measured by the PV simulator. It can be found that the MSBG-inverter can achieve 98.62% MPPT efficiency by using (3.13) without the need of input current sensor and the output power is calculated as 95W. The measured output power curves of two PV panels with different insulations using the proposed MSBG-inverter are shown in Fig. 4.15. PV panel#1 can provide higher power which is calculated as 88W but it is activated later and PV panel#2 can provide lower power which is calculated as 60W. It reveals that the proposed MSBG-inverter can fulfill the DMPPT function for individual PV panel without affecting other one's operation.

doi:10.6342/NTU201603394

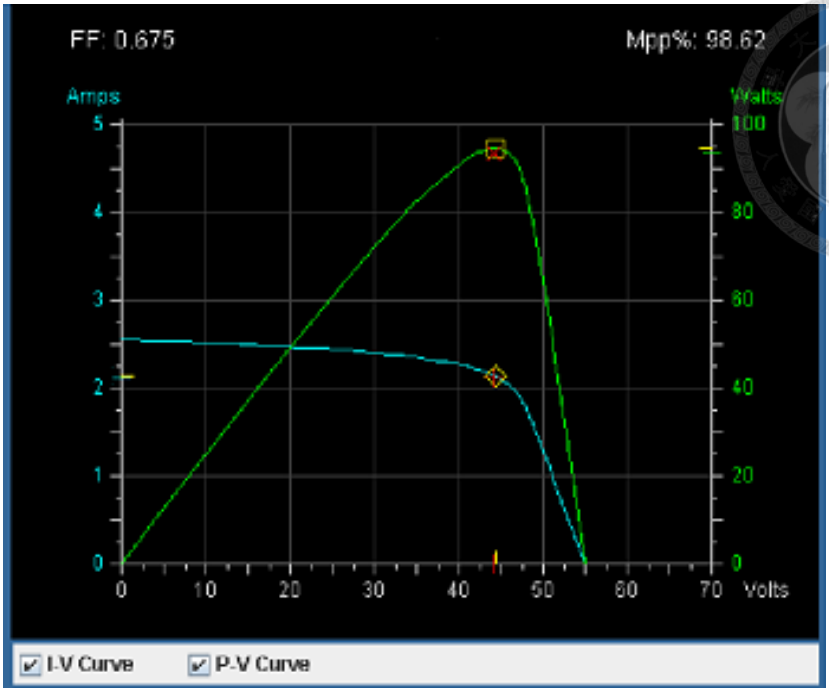

Fig. 4.14 The MPPT efficiency measurement.

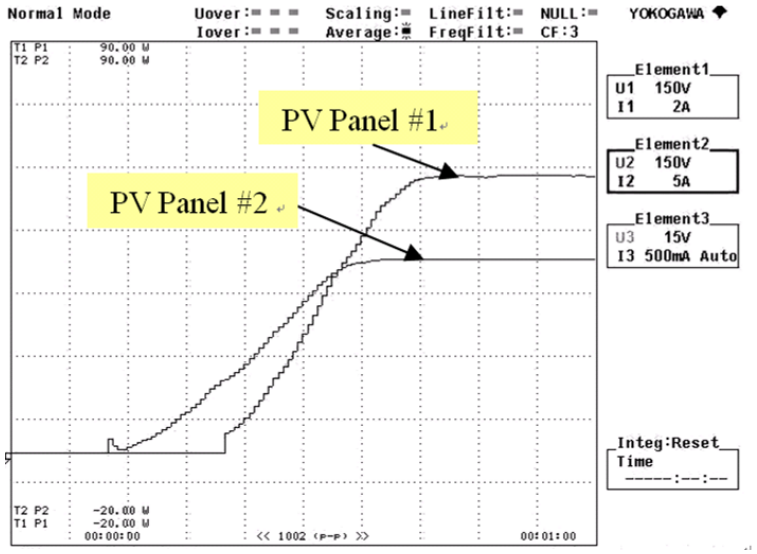

Fig. 4.15 The measured output power curves of two PV panels.

The power conversion efficiency of the proposed MSBG-inverter under different output power is shown in Fig. 4.16. It can be observed that the efficiency is around 92% for a wide PV power range. The picture of the prototype MSBG-inverter is shown in Fig. 4.17.

doi:10.6342/NTU201603394

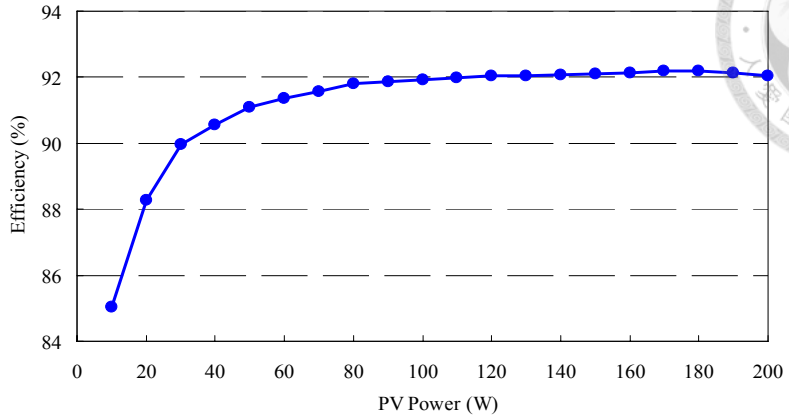

Fig. 4.16 The power conversion efficiency of the proposed MSBG-inverter for the PV system.

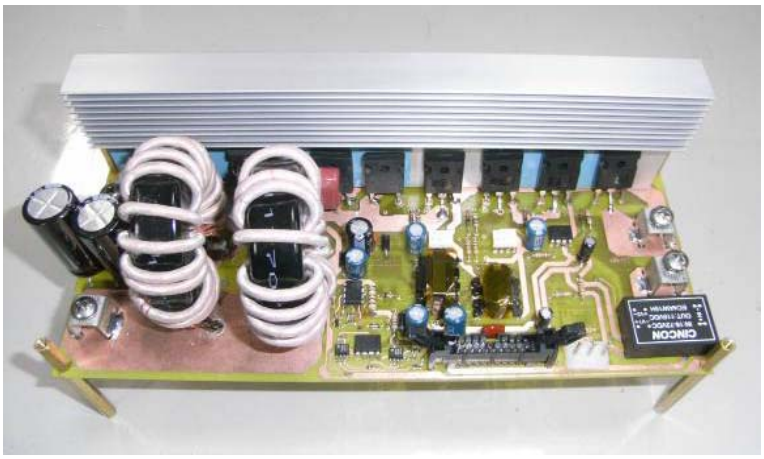

Fig. 4.17 The prototype circuit for the PV system.

4.5 Summary

An MSBG-inverter, which consists of distributed BBCs and an unfolder, for PV system is proposed in this dissertation. The proposed MSBG-inverter can improve the conversion efficiency, increase the overall PV output power, reduce the output inductor size, eliminate the input current sensor, and simplify the control circuit. The distributed BBCs can eliminate the shading effect and fulfill the functions of MPPT as

doi:10.6342/NTU201603394

well as dc-ac conversion. Based on the developed operation principle, the MPPT function can be achieved without the need of input current sensor. Also, with the interleaved operation, the current ripple of the output inductor can be reduced significantly. Computer simulations and hardware measurements are shown to confirm the validity of the proposed MSBG-inverter.

doi:10.6342/NTU201603394

Chapter 5 The MSBG-Inverter for Battery Energy Storage System Applications

Fig. 5.1 shows the block diagram of a conventional battery energy storage system consists of a battery array, which is formed by many battery modules connected in series or parallel, and a bi-directional dc-ac inverter. The total power capacity may be easily reduced by a particular over charging/discharging battery module due to the battery tolerance, unequal battery losses, and so on. In order to maximize energy storage, the energy of the individual battery module connected in series to form a dc bus as the input of the grid-tied inverter must be equalized with each other. The general solution to solve the battery capacity reduction problem is to use extra balancing circuit to connect each battery module and balance the charge of all battery modules. However, the balancing circuit may result in the reduction of total efficiency and the increase of cost and circuit complexity. Also, the high voltage measurement accuracy is required for gauging and battery balancing. The proposed MSBG-inverter is one of the ways to achieve the desired power flow control with balancing the battery modules. Each battery module has its own dc-dc converter to produce a high frequency pulsating dc current with a sinusoidal envelope while the unfolder is realized by an output inductor and four active switches operated at ac line frequency. Therefore, low battery and dc-bus voltages can be accomplished. The pulsating charging/discharging current can help to extend the battery module's lifetime, too. Moreover, expensive current sensors are also eliminated to calculate the battery module output power for the output power control.

doi:10.6342/NTU201603394

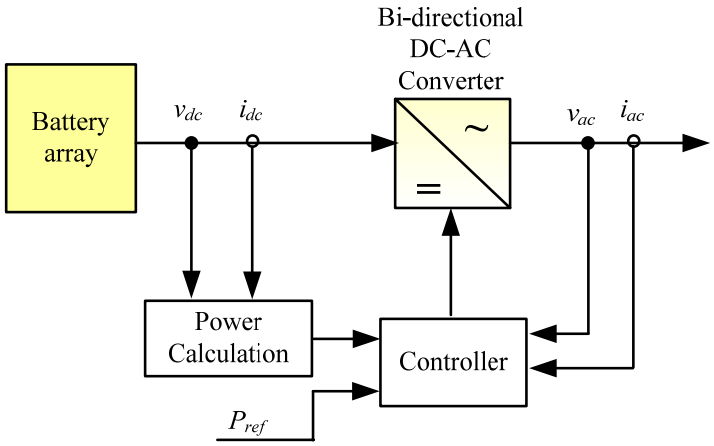

Fig. 5.1 Block diagram of a conventional battery energy storage system [19].

5.1 Battery Module

Based on the power density, battery cost, and battery life consideration, the lead-acid battery and Li-ion battery are the most commonly used energy storage component for the battery energy storage system. Recent developments in Li-ion battery technology show many advantages compared to lead-acid batteries, such as high power and energy density, high working cell voltage, low self-discharge rate, and high charge–discharge efficiency. In the past few decades, ac-impedance analysis has been widely used to explore battery performance including state of charge (SOC) and state of health (SOH). Fig. 5.2 shows the Li-ion battery ac impedance model [46]. This model consists of an ohmic resistance R_o, a double-layer capacitance C_d, a charge transfer resistance R_{ct}, a Warburg impedance Z_w, an anode inductance L_d, and an ideal battery. It can be founded that the individual battery module may have different parameters those usually depend on temperature, SOC, and SOH. In addition, when serially connected, the total battery power capacity may be easily reduced by a particular over charging/discharging battery module due to the temperature, battery tolerance, unequal battery losses, and so on. Therefore, the energy of battery modules must be equalized with each other in order to maximize energy storage for the battery

doi:10.6342/NTU201603394

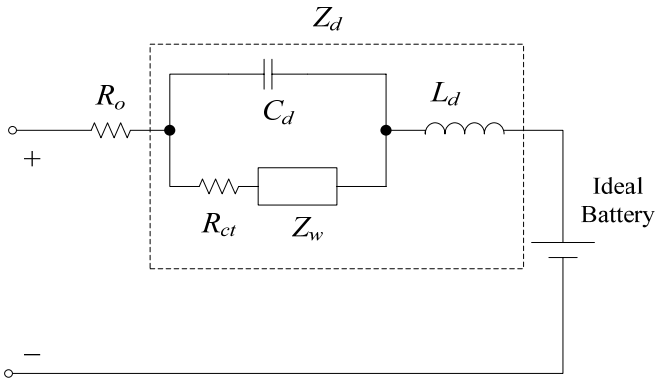

Fig. 5.2 The electrical model of the battery module.

energy storage system.

Another key issue of the battery energy storage system is the life-time of the battery modules. However, the degradation of the electrochemical battery will affect the system's reliability dramatically. It has been reported that the sinusoidal current can improve the Li^+ battery charging efficiency by comparing to the conventional constant-current constant-voltage charging strategy [47]. Also, using pulsating currents to charge/discharge the electrochemical battery can improve the battery efficiency as well as to increase the life-time of the battery [48]. Conventionally, the battery energy storage system needs the two-stages converter to achieve the dc-ac function for the grid-connected inverter and to produce the pulsating charging/discharging current for the battery. Unfortunately, it will reduce the power conversion efficiency of the precious energy storage. Moreover, expensive current sensors are required to calculate the battery module output power for the output power control. Therefore, the MSBG-inverter for battery energy storage system, as shown in Fig. 5.3, is proposed in this dissertation.

doi:10.6342/NTU201603394

5.2 MSBG-Inverter for the Battery Energy Storage System

In Fig. 5.3, each battery module has its own dc-dc converter to control the output power while the unfolder is realized by an output inductor and four active switches operated at ac line frequency. The dc-dc converter produces a high frequency pulsating dc current with a sinusoidal envelope. Therefore, low battery and dc-bus voltages can be accomplished. The pulsating charging/discharging current can help to extend the battery module's lifetime, too. The unfolder can convert the high frequency pulsating dc current generated by the dc-dc converters into a sinusoidal one with utility line frequency. Because the unfolder only switches at the zero crossing of the line voltage, its switching loss can be neglected by comparing to those power switches in the DC-DC converter. Therefore, the energy of each battery module is transferred to the ac mains by means of single-stage power conversion. Because of the single-stage operation, the power conversion efficiency can be improved.

The control block diagram of the first BBC set, as an example, is shown in Fig. 5.4. The discharging/charging and power commands, D/C and P_{i1}, are generated by the BMS and are sent to the controller of the MSBG-inverter. The duty cycle signals, D_{p1} and d_{c1}, can be determined by using the derived equations (3.13) and (3.17). For the battery discharging operation, the unity sinusoidal function with the grid frequency, $|sin\omega t|$, can be via a phase luck loop (PLL) and is used to obtain the reference signal $D_{p1}|sin\omega t|$. The gate signal of S_{d1} can be generated by comparing $D_{p1}sin\omega t$ with the saw-tooth carrier signal V_{sw}. Also, the gate signal of S_{c1} can be generated by comparing the duty cycle d_{c1} with the saw-tooth carrier signal V_{sw} for the battery charging operation.

doi:10.6342/NTU201603394

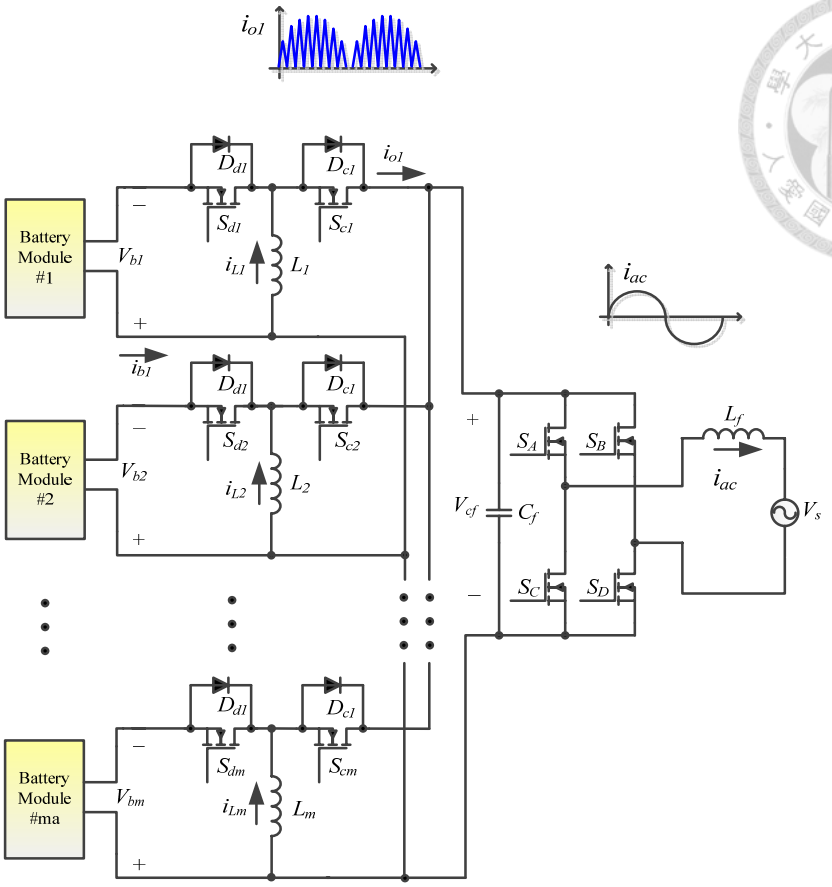

Fig. 5.3 The circuit diagram of the proposed MSBG-inverter for battery energy storage system.

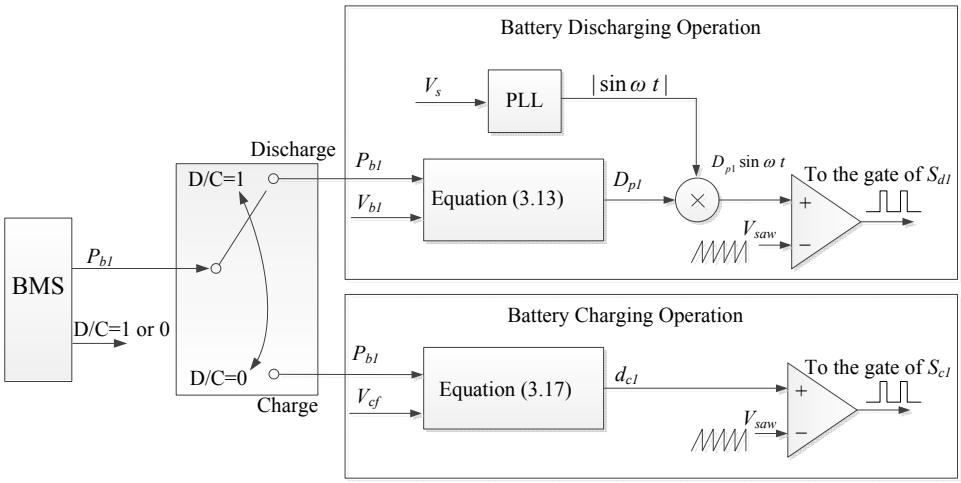

Fig. 5.4 The control block diagram of the proposed MSBG-inverter for the battery energy storage system.

doi:10.6342/NTU201603394

For the battery energy storage system, current sensors are always needed. Conventionally, two current sensors, one for the BMS, which includes the SOC and temperature monitoring, and the other for the power converter, which realizes the current control capability, are demanded for the battery energy storage system. The proposed MSBG-inverter can achieve the desired power flow control without the need of current sensors. Also, it can be adopted for different BMSs as long as the communication protocol for the power flow command is determined.

Eq. (3.13) reveals that the average battery discharging power is only related to V_{b1} and D_{p1} and Eq. (3.17) reveals that the average battery charging power is only related to $V_{cf}[k]$ and d_{c1} if other parameters (f_s, N, and L_1) are carefully designed. Also, the battery discharging/charging power can be determined without measuring the battery current.

Table 5.1 Battery module specifications

Nominal capacity(0.2C)	7 Ah
Rated voltage	48 V
Maximum charging voltage	58 V
Cut-off voltage	40 V
Standard charging and discharging current	0.2 C
Maximum discharging current	1 C

5.3 Computer Simulation and Experimental Verifications

A prototype of the proposed MSBG-inverter with two BBCs is built and tested. To achieve the desired output power, the component values and parameters must match the equations derived in previous sections. The specifications of the battery modules used for the design example are listed in Table 5.1. For the $110V_{ac,rms}$/60Hz utility line, by using (3.6) and (3.12), the maximum duty ratio can be obtained:

doi:10.6342/NTU201603394

$$D_{p1} < 0.756 \quad (5.1)$$

$$d_{d1} < 0.243 \quad (5.2)$$

Consider of the power loss, the turn-off losses and the conduction losses are the primary concerns. To obtain the desired battery module output power, the key components S_{d1} and S_{c1} are both used by MOSFET IRFP360. The conduction loss $P_{d1(conduction)}$ as a function of D_{p1} and $P_{c1(conduction)}$ as a function of d_{c1} are illustrated in Fig. 5.5 from (3.26) and (3.27). It implies that a higher duty ratio is possible in order to reduce the conduction losses. The input inductor L_1 and the turn-off loss $P_{d1(turn\text{-}off)}$ as the functions of the switching frequency f_s can be illustrated in Fig. 5.6 from (3.28) and (3.29). It also implies that a small size inductor is possible and the weight of the proposed MSBG-inverter can be reduced. However, a high switching frequency implies a large switching loss and the trade-off between the inductance reduction and the switching loss increment need to be carefully judged.

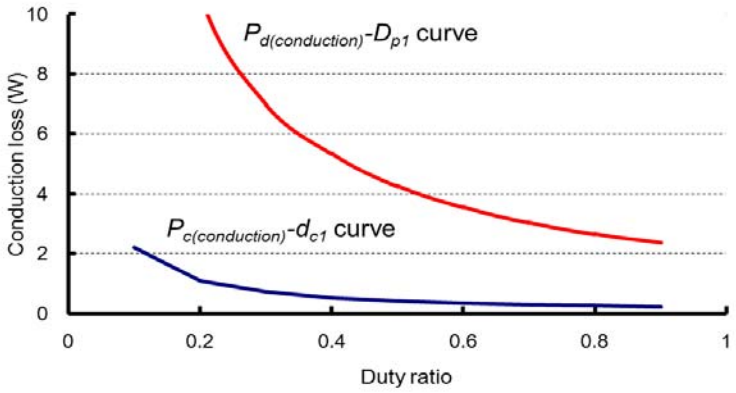

Fig. 5.5 The conduction losses as a function of duty ratio.

doi:10.6342/NTU201603394

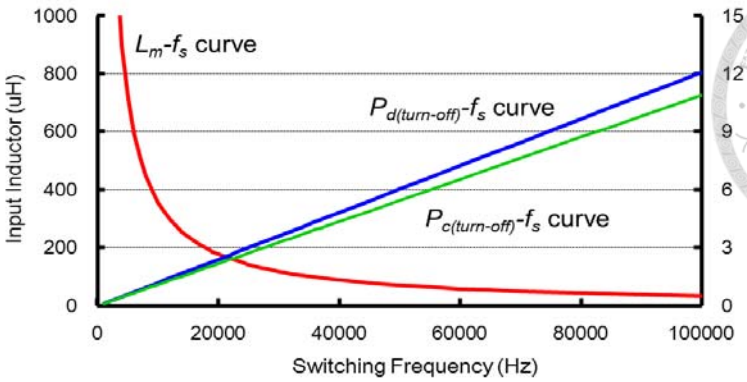

Fig. 5.6 The input inductor L_m and the turn-off loss as the functions of switching frequency f_s.

Based on the derived mathematical equations in previous sections, specifications of the prototype MSBG-inverter can be determined as:

1) Input inductor $L_1 = L_2 = 180$ μH

2) Battery module rating voltage $V_{b1} = 52$V

2) AC mains = 110 Vrms/60Hz

3) Switching frequency $f_s = 20$ kHz

4) Output capacitor $C_f = 2$μF

5) Output inductor $L_f = 1.8$ mH

With the design procedure presented in pervious sections, the output current of the proposed MSBG-inverter can be well controlled. The computer simulation tool Simplis is also used to verify the operation of the proposed MSBG-inverter for the battery energy storage system shown in Fig. 5.7. Fig. 5.8(a) and (b) are the key waveforms of the proposed MSBG-inverter for battery discharging and charging operations, respectively. It is obvious that the input inductor current i_{L1} has an envelope of rectified sinusoidal waveform and an almost sinusoidal output current is

doi:10.6342/NTU201603394

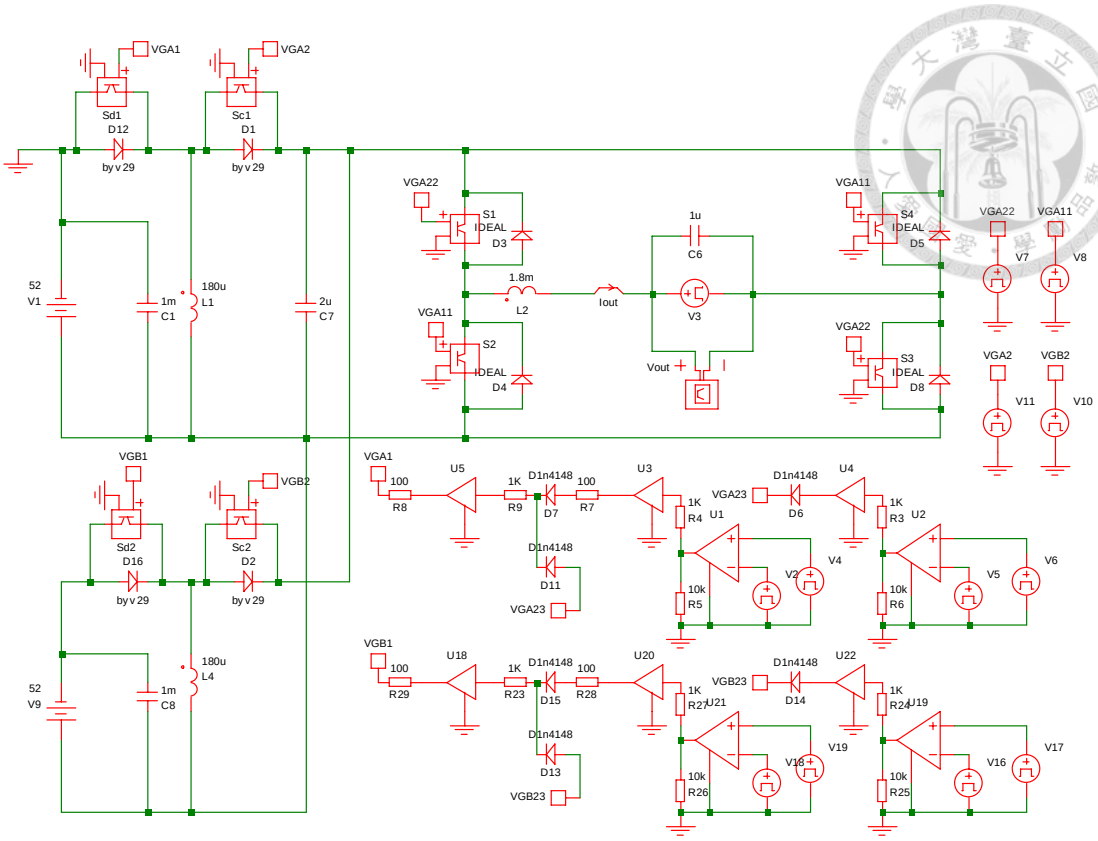

Fig. 5.7 The proposed MSBG-inverter circuit for the battery energy storage system in Simplis.

generated. In Fig. 5.8(a), the output current i_{ac} of the MSBG-inverter has a peak value equal to 1.5A in battery discharging mode and the rms value of the ac mains voltage V_{ac} is 110V. In Fig. 5.8(b), the peak value of output current i_{ac} is reversed in battery charging operation. Also, it is necessary to calibrate the power calculation and determine the effective inductance value after the hardware circuit is implemented.

doi:10.6342/NTU201603394

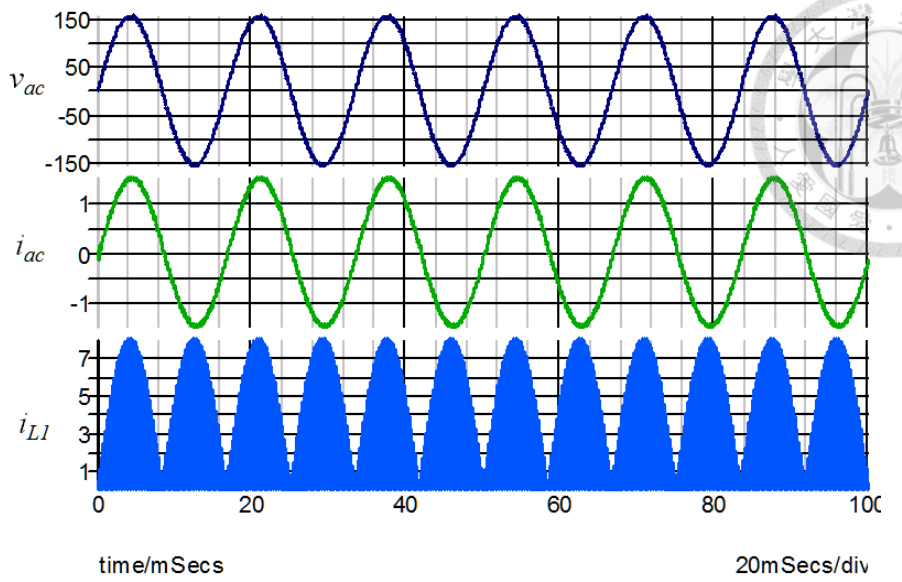

(a) battery discharging operation

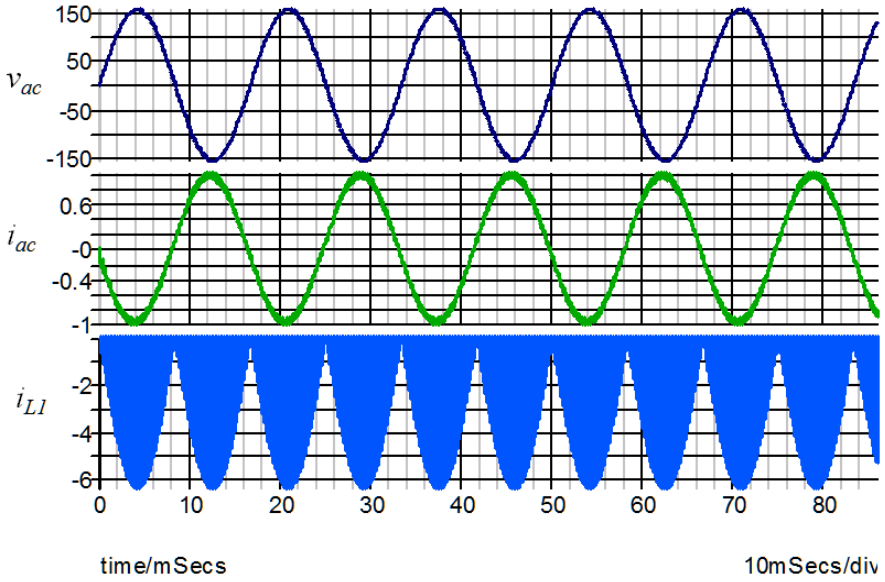

(b) battery charging operation

Fig. 5.8 Computer simulations of ac main voltage (top), ac output current (middle), and input current (bottom) for MSBG-inverter with battery discharging and charging operations.

The corresponding hardware experimental waveforms of the simulated ones are shown in Fig. 5.9. The controller is implemented by microprocessor, TMS320F2808, with the merit of circuit simplicity. Experimental waveforms are consistent with the

doi:10.6342/NTU201603394

simulated ones and the ac output current is almost in phase with the ac mains voltage. The measured total harmonic distortion for the proposed inverter is about 4.9% for the battery discharging operation and 4.3% for the battery charging operation. It should be mentioned that as the number of battery module increase, the ripple current will be reduced due to the nature of interleaved operation. Therefore, a lower current THD can be expected.

Another important feature of the proposed inverter is the individual power-handling capability without the need of input current sensor. The measured output power curves of two battery modules with different insulations using the proposed MSBG-inverter are shown in Fig. 5.10. Battery module#1 can provide higher power which is calculated as 95W and battery module#2 can provide lower power which is calculated as 60W. It reveals that the proposed MSBG-inverter can control the power for individual battery module without affecting other one's operation. The power conversion efficiency of the proposed MSBG-inverter under different output power is shown in Fig. 5.11. It can be observed that the efficiency is also around 92% for a wide charging/discharging power range. The picture of the prototype MSBG-inverter is shown in Fig. 5.12.

doi:10.6342/NTU201603394

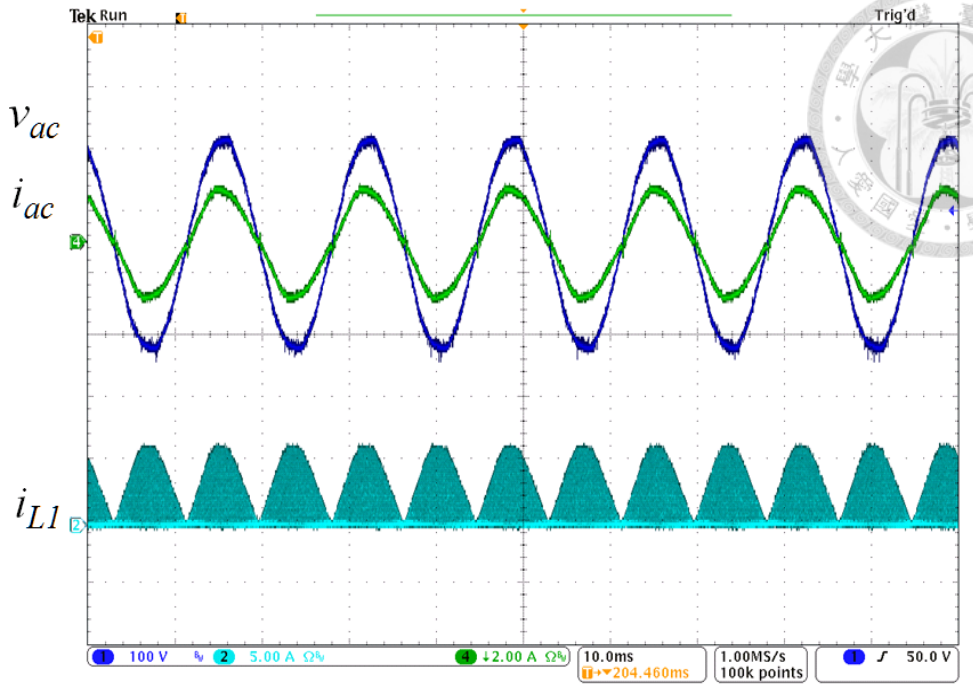

(a) battery discharging operation

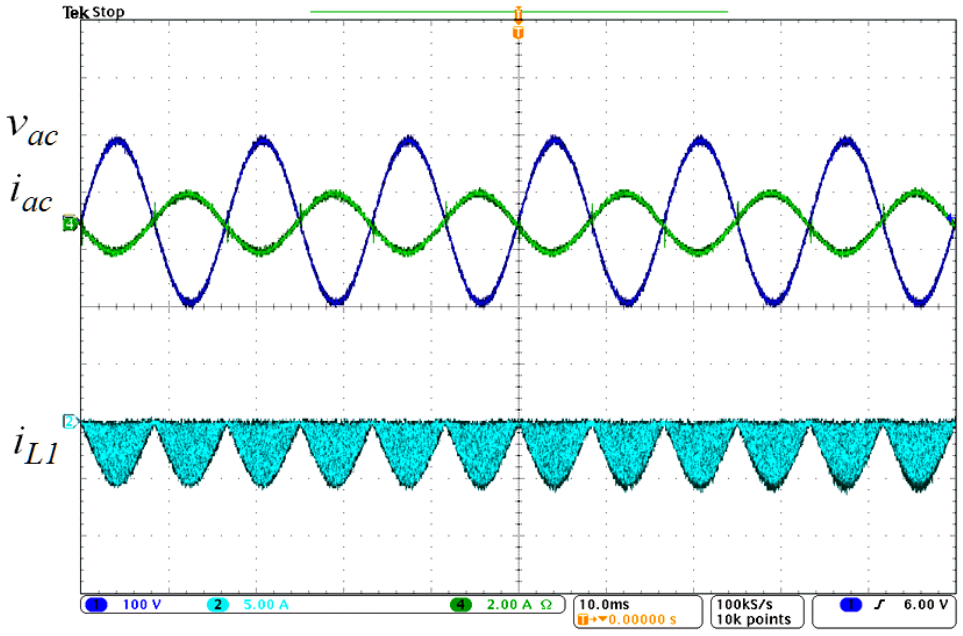

(b) battery charging operation

Fig. 5.9 Experimental waveforms of ac main voltage, ac output current, and input current for MSBG-inverter with battery discharging and charging operations.

doi:10.6342/NTU201603394

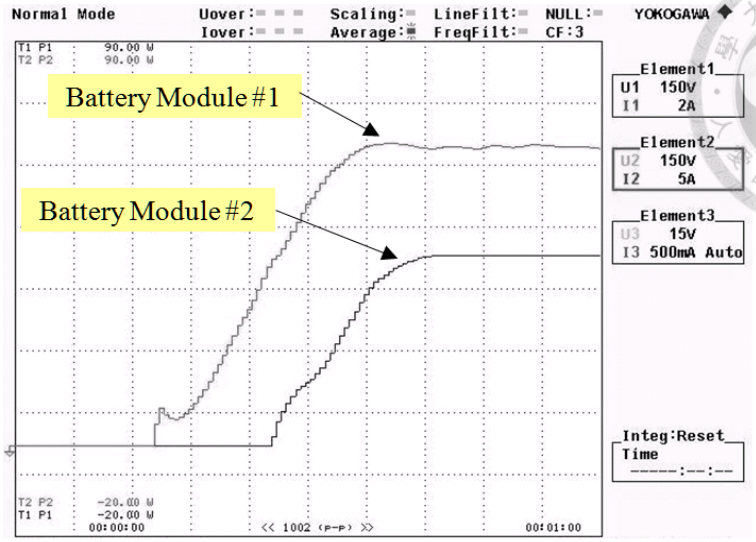

Fig. 5.10 The measured output power curves of two battery modules with different power commands.

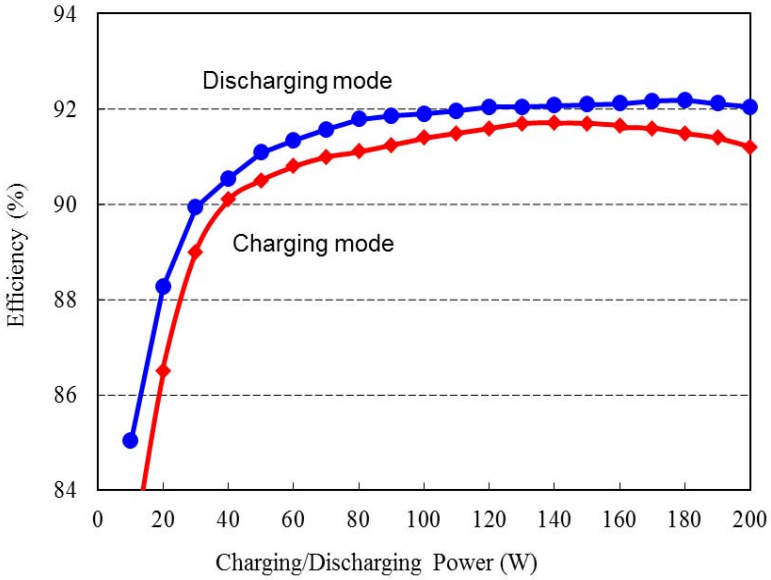

Fig. 5.11 The power conversion efficiency of the proposed MSBG-inverter.

doi:10.6342/NTU201603394

Fig. 5.12 The prototype circuit for the battery energy storage system.

5.4 Summary

An MSBG-inverter, which consists of distributed BBCs and an unfolder, for battery energy storage system is proposed in this dissertation. Advantages of the proposed MSBG-inverter for the battery energy storage system include: single-stage power conversion, low battery and dc-bus voltages, pulsating charging/discharging currents, and individual power control for each battery module. Therefore, the equalization, lifetime extension, and capacity flexibility of the battery energy storage system can be achieved. Based on the developed equations, the power flow of the battery system can be controlled without the need of input current sensor. Also, with the interleaved operation between BBCs, the current ripple of the output inductor can be reduced too. The computer simulations and hardware experimental results are shown to verify the performance of the proposed MSBG-inverter.

doi:10.6342/NTU201603394

Chapter 6 Conclusions and Suggested Future Research

6.1 Summary and Major Contributions

The objective of this dissertation is to analyze the proposed an MSBG-inverter. The major contribution of the dissertation can be summarized as follows:

1. A prototype of the proposed MSBG-inverter with two BBCs is built and tested for the PV system and the battery energy storage system in this dissertation.
2. Based on the circuit design and the developed equations, the proposed MSBG-inverter has several advantages:
   (a) Individual power-handling (DMPPT),
   (b) Elimination of the input current sensor,
   (c) Reduction of the output inductor (interleaving fashion),
   (d) Improvement of the battery life-time for the battery energy storage system,
   (e) Simplicity of the control circuit, and
   (f) High flexibility for capacity extension
3. The design procedure including the circuit parameters design of the proposed MSBG-inverter has been proposed for the PV system and the battery energy storage system.

6.2 Suggestions for Future Research

In addition to the study addressed in the dissertation, suggested research topics are listed as follows:

1. In this dissertation, a prototype of the proposed MSBG-inverter with two BBCs is built and tested. In the future, the proposed MSBG-inverter with larger numbers of BBCs can be developed to confirm the validity for different PV

doi:10.6342/NTU201603394

panels and battery modules. Also, design of an optimize number of interleaving BBCS is suggested for system efficiency improvement.

2. One of the features of the proposed MSBG-inverter is to improve the power conversion efficiency of the circuit. However, the experimental result shows that the maximum power conversion efficiency of the proposed MSBG-inverter is around 92% which is not good enough and needs some extension. Moreover, switches operating in a complementary fashion can reduce the conduction losses in these types of inverters. However, it requires an extra circuit or a method to detect the inductor current and to turn-off the complementary switch in DCM operation if the complementary fashion is used. Therefore, the analysis of the circuit design, for improving power conversion efficiency is suggested.
3. The accuracy of the power control could be influenced by tolerance or variation of the inductor value, as shown in the power equations (3.14) and (3.17). Hence, it is necessary to calibrate the power calculation and determine the effective inductance value after the hardware circuit is implemented. If the power calculation can be recalibrated while the BMS detect a severe mismatch between the battery output power and the power command, the problem of component value variation over time could be solved.
4. In this dissertation, the proposed MSBG-inverter is for single phase system. In the future, a three-phase MSBG-inverter can be developed. Therefore, higher capacity application can provide the power condition capability for PV system and battery energy storage system.

doi:10.6342/NTU201603394

References

[1] J.-S. Lai, “Power conditioning systems for renewable energies,” in *International Conference on Electrical Machines and Systems, ICEMS 07*, pp. 209-218, Oct. 2007.

[2] J. P. Benner and L. Kazmerski, “Photovoltaics gaining greater visibility,” *IEEE Spectrum*, vol. 29, no. 9, pp. 34–42, Sep. 1999.

[3] M. Meinhardt and G. Cramer, “Past, present and future of grid connected photovoltaic- and hybrid-power-systems,” in *Proc. IEEE-PES Summer Meeting*, vol. 2, 2000, pp. 1283–1288.

[4] S. B. Kjaer, J. H. Pedersen, and F. Blaabjerg, “A review of single-phase grid-connected inverters for photovoltaic modules,” *IEEE Trans. Ind. Appl.*, vol. 41, no. 5, pp. 1292–1306, Sep. 2005.

[5] M. Hoeven, “Technology Roadmap, Solar Photovoltaic Energy,” International Energy Agency, https://www.iea.org/publications/freepublications/publication/TechnologyRoadmapSolarPhotovoltaicEnergy_2014edition.pdf, 2014.

[6] H. Kanchev , D. Lu , F. Colas , V. Lazarov and B. Francois "Energy management and operational planning of a microgrid with a PV-based active generator for smart grid applications", *IEEE Trans. Ind. Electron.*, vol. 58, no. 10, pp.4583 -4592 2011

[7] Z. Zhao, M. Xu, Q. L. Chen, J. S. Lai, and Y. Cho, “Derivation, analysis, and implementation of a boost-buck converter-based high-efficiency PV inverter,”

doi:10.6342/NTU201603394

IEEE Trans. Power Electron., vol. 27, no. 3, pp. 1304–1313, Mar. 2012.

[8] E. Koutroulis and F. Blaabjerg, "Design optimization of transformerlwss grid-connected PV inverters including reliability," *IEEE Trans. Power Electron.*, vol. 28, no. 1, pp. 325–335, Jan. 2013.

[9] L. Zhang, K. Sun, Y. Xing, and M. Xing, "H6 transformerless full-bridge PV grid-tied inverters," *IEEE Trans. Power Electron.*, vol. 29, no. 3, pp. 1229–1238, Mar. 2014.

[10] Sreeraj. E. S., K. Chatterjee, and S. Bandyopadhyay, "One-cycle-controlled single-stage single-phase voltage-sensorless grid-connected PV system," *IEEE Trans. Ind. Electron.*, vol. 60, no. 3, pp. 1216–1224, Mar. 2013.

[11] Y. Tang, X. Dong, and Y. He, "Active buck-boost inverter," *IEEE Trans. Ind. Electron.*, vol. 61, no. 9, pp. 4691–4697, Sep. 2014.

[12] S. Jiang, D. Cao, Y. Li, and F. Z. Peng, "Grid-connected boost-half-bridge photovoltaic microinverter system using repetitive current control and maximum power point tracking," *IEEE Trans. Power Electron.*, vol. 27, no. 11, pp. 4711–4722, Nov. 2012.

[13] E. Kourtroulis, K. Kalaitzakis, and N. C. Voulgaris, "Development of a microcontroller-based, photovoltaic maximum power point tracking control system," *IEEE Trans. Power Electron.*, vol. 16, no. 1, pp. 46-54, 2001.

[14] Y. H. Ji, D. Y. Jung, J. G. Kim, J. H. Kim, T. W. Lee, and C. Y. Won, "A real maximum power point tracking method for mismatching compensation in PV array under partially shaded conditions," *IEEE Trans. Power Electron.*, vol. 26, no. 4, pp. 1001–1009, Apr. 2011.

[15] G. Carannante, C. Fraddanno, and M. Pagano, "Experimental performance of MPPT algorithm for photovoltaic sources subject to inhomogeneous insolation,"

doi:10.6342/NTU201603394

IEEE Trans. Ind. Electron., vol. 56, no. 11, pp.4374-4380, Nov.2009.

[16] B. N. Alajmi, K. H. Ahmed, S. J. Finney, and W. Williams, "A maximum power point tracking technique for partially shaded photovoltaic systems in microgrids," *IEEE Trans. Ind. Electron.*, vol. 60, no. 4, pp.1596-1606, Apr. 2013.

[17] M. Boztepe, F. Guinjoan, G. V. Quesada, S. Silvestre, A. Chouder, and E. Karatepe, "Global MPPT scheme for photovoltaic string inverters based on restricted voltage window search algorithm," *IEEE Trans. Ind. Electron.*, vol. 61, no. 7, pp.3302-3312, Jul. 2014.

[18] J. Y. Kim, J. H. Jeon, S. K. Kim, C. Cho, J. H. Park, H.-M. Kim, and K.Y. Nam, "Cooperative control strategy of energy storage system and microsources for stabilizing the microgrid during islanded operation," *IEEE Trans. Power Electron.*, vol. 25, no. 12, pp. 3037-3048, Dec. 2010.

[19] H. Qian, J. Zhang, J. S. Lai, and W. Yu, "A high-efficiency grid-tie battery energy storage system," *IEEE Trans. Power Electron.*, vol. 26, no. 3, pp. 886-896, 2011.

[20] J. He and Y. W. Li, "Hybrid voltage and current control approach for DG-grid interfacing converters with LCL filters," *IEEE Trans. Ind. Electron.*, vol. 60, no. 5, pp.1797-1809, Mar. 2013.

[21] M. Y. Kim, C. H. Kim, J. H. Kim, and G. W. Moon, "A chain structure of switched capacitor for improved cell balancing speed of lithium-ion batteries," *IEEE Trans. Ind. Electron.*, vol. 61, no. 8, pp. 3989-3999, Aug. 2014.

[22] K. M. Lee, Y. H. Chung, C. H. Sung, and B. Kang, "Active cell balancing of Li-ion batteries using LC series resonant circuit," *IEEE Trans. Ind. Electron.*, vol. 62, no. 9, pp. 5491-5501, Sep. 2015.

[23] W. Huang and A. Qahouq, "Energy Sharing Control Scheme for State-of-Charge

doi:10.6342/NTU201603394

Balancing of Distributed Battery Energy Storage System," *IEEE Trans. Ind. Electron.*, vol. 62, no. 5, pp. 2764-2776, May 2015.

[24] C. L. Chen, Y. Wang, J. S. Lai, and Y. S. Lee, "Design of parallel inverters for smooth mode transfer microgrid applications," *IEEE Trans. Power Electron.*, vol. 25, no. 1, pp. 6-14, 2010.

[25] N. Mukherjee and D. Strickland, "Control of second-life hybrid battery energy storage system based on modular boost-multilevel buck converter," *IEEE Trans. Ind. Electron.*, vol. 62, no. 2, pp.1034-1046, Feb. 2015.

[26] C. W. Chen, K. H. Chen, and Y. M. Chen, "Modeling and controller design of an autonomous PV module for DMPPT PV systems," *IEEE Trans. Power Electron.*, vol. 29, no. 9, pp. 4723–4732, Sep. 2014

[27] A. I. Bratcu, I. Munteanu, S. Bacha, D. Picault, and B. Raison, "Cascaded DC-DC converter photovoltaic system: Power optimization issues," *IEEE Trans. Ind. Electron.*, vol. 58, no. 2, pp. 403–411, Feb. 2011.

[28] S. Poshtkouhi, V. Palaniappan, and O. Trescases, "A general approach for quantifying the benefit of distributed power electronics for fine grained MPPT in photovoltaic applications using 3-D modeling," *IEEE Trans. Power Electron.*, vol. 27, no. 11, pp. 4656–4666, Nov. 2012.

[29] Z. Liang, R. Guo, J. Li, and A. Q. Huang, "A high-efficiency PV module-integrated DC/DC converter for PV energy harvest in FREEDM systems," *IEEE Trans. Power Electron.*, vol. 26, no. 3, pp. 897–909, Mar. 2011.

[30] L. Maharjan, T. Yamagishi, and H. Akagi, "Active-power control of individual converter cells for a battery energy storage system based on a multilevel cascade PWM converter," *IEEE Trans. Power. Electron.*, vol. 27, no. 3, pp.1099-1107, Mar. 2012.

doi:10.6342/NTU201603394

[31] M. Vasiladiotis and A. Rufer, “A modular multiport power electronic transformer with integrated split battery energy storage for versatile ultrafast EV charging stations,” *IEEE Trans. Ind. Electron.*, vol. 62, no. 5, pp. 3213-3222, May 2015.

[32] H. Hu, S. Harb, N. H. Kutkt, Z. J. Shen, and I. Batarseh, “A single-stage microinverter without using electrolytic capacitors,” *IEEE Trans. Power Electron.*, vol. 28, no. 6, pp. 2677–2687, Jun. 2013.

[33] N. Sukesh, M. Pahlevaninezhad, and P. K. Jain, “Analysis and implementation of a single-stage Flyback PV microinverter with soft switching,” *IEEE Trans. Ind. Electron.*, vol. 61, no. 4, pp. 1819–1833, Apr. 2014.

[34] W. J. Cha, Y. W. Cho, and B. H. Kwon, “Highly efficient microinverter with soft-switching step-up converter and single-switch-modulation inverter,” *IEEE Trans. Ind. Electron.*, vol. 62, no. 6, pp. 3516–3523, Jun. 2015.

[35] A. Nabae, I. Takahashi, and H. Akagi, “A New Neutral-Point-Clamped PWM Inverter”, *IEEE Trans. Ind. Appl.*, vol. IA-17, no. 5, pp.518-523, 1981.

[36] H. R. Teymour, D. Sutanto, K. M. Muttaqi, and P. Ciufo, “Solar PV and Battery Storage Integration using a New Configuration of a Three-Level NPC Inverter With Advanced Control Strategy,” *IEEE Trans. Energy Conver.*, vol. 29, no. 2, pp. 354–365, Jun. 2014.

[37] M. Victor, F. Greizer, S. Bremicker, and U. Huebler, “Europeische Patentanmeldung,” EP 1 626 494 A2.

doi:10.6342/NTU201603394

[38] H. Schmidt, Ch. Siedle, and J. Ketterer, “Europeische Patentanmeldung,” EP 1 369 985 A2.

[39] W. Li, Y. Gu, H. Luo. W. Cui, X. He, and C. Xia, “Topology review and derivation methodology of single-phase transformerless photovoltaic inverters for leakage current suppression,” *IEEE Trans. Ind. Electron.*, vol. 62, no. 7, pp. 4537-4551,Jul. 2015.

[40] R. J. Wai, C. Y. Lin, and Y. R. Chang, “Novel maximum-power-extraction algorithm for PMSG wind generation system,” *IET Electric Power Appl.*, vol. 1, no. 2, pp. 275–283, Mar. 2007.

[41] R. M. Santos Filho, P. F. Seixas, P. C. Cortizo, L. A. B. Torres, and A. F. Souza, “Comparison of three single-phase PLL algorithms for UPS applications,” *IEEE Trans. Ind. Electron.*, vol. 55, no. 8, pp. 2923–2932, Aug. 2008.

[42] F. D. Freijedo, J. Doval-Gandoy, Ó. López, and E.Acha, “Tuning of phaselocked loops for power converters under distorted utility conditions,” *IEEE Trans. Ind. Appl.*, vol. 45, no. 6, pp. 2039–2047, Nov./Dec. 2009.

[43] D. Graovac , M. Purschel and A. Kiep, “MOSFET power losses calculation using the data-sheet parameters”, *Infineon Application Note*, 2006.

[44] SW 285 MONO datasheet, SOLARWORLD, 2014.

doi:10.6342/NTU201603394

[45] H. Hu, S. Harb, N. H. Kutkut, Z. J. Shen and I. Batarseh, "A single-stage microinverter without using eletrolytic capacitors", *IEEE Trans. Power Electron.*, vol. 28, no. 6, pp. 2677-2687, 2013.

[46] S. Buller, M. Thele, R.W. A. A. D. Doncker, and E. Karden, “Impedancebased simulation models of supercapacitors and Li-ion batteries for power electronic applications,” *IEEE Trans. Ind. Appl*., vol. 41, no. 3, pp. 742–747, Jun. 2005.

[47] M. Coleman, C. K. Lee, C. Zhu, and W. G. Hurley, “State-of-charge determination from EMF voltage estimation: Using impedance, terminal voltage, and current for lead–acid and lithium-ion batteries,” *IEEE Trans. Ind. Electron.*, vol. 54, no. 5, pp. 2550–2557, Oct. 2007.

[48] L. R. Chen, J. J. Chen, C. M. Ho, S. L. Wu, and D. T. Shieh, “Improvement of Li-ion battery discharging performance by pulse and sinusoidal current strategies,” *IEEE Trans. Ind. Electron.*, vol. 60, no. 12, pp. 5620-5628, Dec. 2013.

[49] L. R. Chen, S. L. Wu, D. T. Shieh, and T. R. Chen, “sinusoidal-ripple-current charging strategy and optimal charging frequency study for Li-ion batteries,” *IEEE Trans. Ind. Electron.*, vol. 60, no. 1, pp. 88-97, Jan. 2013.

doi:10.6342/NTU201603394

[50] J. Li, E. Murphy, J. Winnick, and P. A. Kohl, “The effects of pulse charging on cycling characteristics of commercial lithium-ion batteries,” *Journal of Power Sources*, no. 102, pp.302-309, 2001.

[51] N. Kasa, T. Iida, and L. Chen, “Flyback inverter controlled by sensorless current MPPT for photovoltaic power system,” *IEEE Trans. Ind. Electron.*, vol. 52, no. 4, pp. 1145-1152, 2005.

[52] Y. M. Chen, K. Y. Lo, and Y. R. Chang, “Multi-string single-stage grid-connected inverter for PV system,” in *Proc. ECCE*, 2011, pp. 2751–2756.

[53] H. Patel and V. Agarwal, “A single-stage single-phase transformer-less doubly grounded grid-connected PV interface,” *IEEE Energy Convers.,* vol. 24, no. 1, pp. 93-101, Mar. 2009.

[54] F. Tian, S. Kasemsan, and, I. Batarseh, “An adaptive slope compensation for the single-stage inverter with peak current-mode control,” *IEEE Trans. Power Electron.*, vol. 26, no. 10, pp. 2857-2862, Oct. 2011.

[55] D. Meneses, F. Blaabjerg, O. Garcia, and J. A. Cobos, “Review and comparison of step-up transformerless topologies for photovoltaic AC-module application,” *IEEE Trans. Power Electron.*, vol. 28, no. 6, pp. 2649–2663, Jun. 2013.

[56] S. M. MacAlpine, R. W. Erickson, and M. J. Brandemuehl, “Charaterization of power optimizer potential to increase energy capture in photovoltaic systems operating under nonuniform conditions,” *IEEE Trans. Power Electron.*, vol. 28, no. 6, pp. 2936–2945, Jun. 2013.

doi:10.6342/NTU201603394

[57] Y. Xue, L. Chang, S. J. Kjær, J. Bordonau, and T. Shimizu, "Topologies of single-phase inverters for small distributed power generators: An overview," *IEEE Trans. Power Electron.*, vol. 19, no. 5, pp. 1305-1314, Sep. 2004.

[58] Q. Li and P.Wolfs, "A review of the single phase photovoltaic module integrated converter topologies with three different DC link configurations," *IEEE Trans. Power Electron.*, vol. 23, no. 3, pp. 1320–1333, May 2008.

[59] P. Tsao, S. Sarhan, and I. Jorio, "Distributed maximum power point tracking of photovoltaic arrays: Novel approach and system analysis," *IEEE Trans. Ind. Electron.*, vol. 55, no. 7, pp.2610-2621, 2008.

[60] Y. Fang, and X. Ma, "A novel PV microinverter with coupled inductors and double-boost topology," *IEEE Trans. Power Electron.*, vol. 25, no. 12, pp. 3139–3147, Dec. 2010.

doi:10.6342/NTU201603394

Vita

Kuo-Yuan Lo was born in Taichung, Taiwan, in 1981. He received the B.S. degree in electrical engineering from the National Taipei University of Technology, Taipei, Taiwan, in 2003 and received the M.S. degree in electrical engineering from the National Cheng-Kung University, Tainan, Taiwan, in 2006. He is currently pursuing the Ph. D. degree in electrical engineering at National Taiwan University, Taipei, Taiwan. His research interests include grid-connected inverters and microgrid applications.

Publications

- ***Major Journal***

[1] **K.-Y. Lo**, Y.-M. Chen, and Y.-R. Chang, "Bi-directional single-stage grid-connected inverter for battery energy storage system," *IEEE Trans. on Ind. Electron.*, Early Access Articles.

[2] **K.-Y. Lo**, Y.-M. Chen, and Y.-R. Chang, "MPPT Battery Charger for Stand-Alone Wind Power System," *IEEE Trans. on Power Electron.*, vol.26, no.6, pp.1631-1638, Oct. 2011.

- ***International Conference***

[1] J.-J. Jheng, M.-F. Shih, and **K.-Y. Lo**, "Battery charger with MPPT function for stand-alone wind turbines," in *Proc. IPEMC-ECCE Asia*, 2016, pp.2972-2977.

[2] L.-Y. Liu, M.-C. Tsai, C.-L. Hsu, **K.-Y. Lo**, and Y.-R. Chang, "Design of an energy storage converter for microgrid applications," in *Proc. ICRERA*, 2015, pp.305-310.

doi:10.6342/NTU201603394

[3] Y.-M. Chen, **K.-Y. Lo**, and Y.-R. Chang, "Multi-string single-stage grid-connected inverter for PV system," in *Proc. IEEE ECCE,* 2011, pp.2751-2756.

[4] **K.-Y. Lo**, Y.-M. Chen, and Y.-R. Chang, "Battery charger with MPPT function for stand-alone wind turbines," in *Proc. IPEC,* 2010, pp.932-937.

- ***Patent***

[1] K.-Y. Lo, Y.-R. Chang, and Y.-M. Chen, “Household Grid-Connected Inverter Applied to Solar Power Generation System with Maximum Power Tracking Function,” U.S. Patent Pending, 13/607,044, Mar. 2014.

[2] 羅國原、張永瑞、陳耀銘， “應用於太陽發電系統並具有最大功率追蹤之市電並聯換流器,” 中華民國專利號 I487239, 2015.

[3] 羅國原、張永瑞、陳耀銘， “用於風力發電機之充電裝置,” 中華民國專利號 I390819, 2013.

doi:10.6342/NTU201603394